Correspondence to:

I. V. Sleptsova and S. A. Gilder,
iu.sleptsova@lmu.de;
gilder@lmu.de

Thermal and Structural History of Impact Ejecta Deposits, Ries Impact Structure, Germany

Iuliia V. Sleptsova[1] [ID], **Stuart A. Gilder[1]** [ID], **Fabian Dellefant[1], Claudia A. Trepmann[1], Nastaran Ahanin[1], and Jean Pohl[1]**

[1]Department of Earth and Environmental Sciences, Ludwig-Maximilians-University, Munich, Germany

Abstract The Ries impact structure (Germany) contains well-preserved ejecta deposits consisting of melt-free lithic breccia (Bunte Breccia) overlain by suevite. To test their emplacement conditions, we investigated the magnetic properties and microstructures of 26 polymict breccia clasts and a stratigraphic profile from the clasts into the suevite at the Aumühle quarry. Remanent magnetization directions of the Bunte Breccia clasts fall into two groups: those whose directions mostly lie parallel to the reversed field during impact carried mostly by magnetite, and those whose directions vary widely among each clast carried by titanohematite. Basement clasts containing titanohematite acquired a chemical remanent magnetization (CRM) during the ejection process and then rotated during turbulent deposition. Clasts of sedimentary rocks grew magnetite after turbulent deposition, with CRM directions lying parallel to the paleofield. Suevite holds a thermal remanent magnetization carried by magnetite, except for ∼12 cm from the contact with the Bunte Breccia, where hematite concentrations increase due to hydrothermal alteration. These observations lead us to propose a three-stage model of (a) turbulent deposition of the melt-free breccia with clast rotation <580°C, (b) deposition of the overlying suevite, which acted as a semi-permeable barrier that confined hot (<300°C) oxidizing fluids to the permeable breccia zone, and (c) prolonged hydrothermal activity producing further alteration which ended before the next geomagnetic reversal. Basement outcrops have significantly different magnetic properties than the Bunte Breccia basement clasts with similar lithology. Two basement blocks situated near the inner ring may have been thermally overprinted up to 550°C.

Plain Language Summary The 26-km-diameter, ∼15-million-year-old Ries meteorite impact structure in southern Germany is characterized by well-preserved ejecta deposits expelled from the crater within seconds after the impact. These deposits consist of two main layers: melt-free, lithic breccia (Bunte Breccia), overlain by melt-bearing breccia (suevite). To understand the formation conditions of the ejecta deposits, we performed paleomagnetic and rock magnetic measurements and microstructural experiments on clasts within Bunte Breccia and on the overlying suevite at the Aumühle quarry. We found that clasts derived from crystalline basement materials experienced high pressures during the impact. These clasts had randomly oriented magnetization directions carried by titanohematite. In contrast, clasts derived from sedimentary rocks experienced only low pressures and had coherent magnetization directions oriented parallel to the reversed field during the impact that are carried by magnetite. Our findings can be interpreted by a three-stage model that explains the thermal and structural formation of impact ejecta at the Ries impact structure.

1. Introduction

Meteorite impact structures are a common feature in celestial bodies throughout our solar system. Although >200 terrestrial craters have been documented in the geologic record (Kenkmann, 2021; Osinski et al., 2022), erosion and tectonic activity continually act to eliminate or obscure them, so their presence over Earth's history is underestimated. Despite the importance for the Earth and planetary sciences, many aspects of crater formation remain poorly understood. Moreover, widespread hydrothermal activity is commonly observed at impact structures, for example, Chixculub (Kring et al., 2020), Haughton (Zylberman et al., 2017), Karla (Kuzina et al., 2022), and Ries (Arp et al., 2013; Muttik et al., 2010; Osinski, 2005). These environments have been proposed to be ideal for initiating and sustaining early life (Kring et al., 2020; Osinski et al., 2013), yet the duration of hydrothermal systems is poorly constrained.

When an asteroid or comet hits a solid rock surface at ∼20 km/s, the target rocks are affected by a shock wave. Pressures can reach a few hundred GPa during the compression stage, accompanied by temperatures exceeding

Writing – original draft: Iuliia V. Sleptsova, Stuart A. Gilder
Writing – review & editing: Iuliia V. Sleptsova, Stuart A. Gilder, Fabian Dellefant, Claudia A. Trepmann, Nastaran Ahanin, Jean Pohl

10,000°C causing the material to vapourize, while farther away, the target rocks melt and often resemble volcanic deposits when redeposited on the surface (e.g., Collins et al., 2012; Melosh, 1989; Stöffler et al., 2018). Some of the material is ballistically expelled from the transient crater, forming a blanket of impact ejecta. Variations in target rock composition and complicated excavation processes lead to highly heterogeneous impact ejecta.

The Ries impact structure (Germany) provides an excellent opportunity to study well-exposed polymict breccia ejecta deposits (e.g., Hüttner & Schmidt-Kaler, 1999; Pohl et al., 1977; Stöffler et al., 2013; Sturm et al., 2015): (a) the Bunte (German for "varicolored") Trümmermassen (German for "debris masses") composed of melt-free lithic breccia (Bunte Breccia, ejecta sized <25 m in diameter) and allochthonous megablocks (ejecta sized >25 m) and (b) overlying suevite composed of melt-fragment-bearing (glass, etc.) breccia (Figure 1). As detailed below, considerable research has focused on suevite, whereas much less is known about the Bunte Trümmermassen; moreover, the contact relationship between the two is seldom documented (e.g., von Engelhardt et al., 1995). To better determine the emplacement conditions of the Bunte Trümmermassen and its relationship to the overlying suevite, we investigated the magnetic properties and microfabrics of clasts in a horizon rich in crystalline basement and sedimentary clasts and a stratigraphic profile from the clasts into the suevite at the Aumühle quarry, where a continuous exposure between the two is clearly visible (Figures 1b and 2a). We compare the magnetic properties of the clasts entrained in the Bunte Breccia with analogous lithologies around the crater outside the quarry (Figure 1a).

2. Geological Setting and Sampling

The Ries crater is a complex meteorite impact structure located in southern Germany (48°53′N, 10°37′E; Figure 1a). Its diameter is estimated to be 26 km, with a 12 km diameter inner ring composed mainly of a crystalline basement surrounded by an annular zone bounded by concentric normal faults that form the structural crater rim (Pohl et al., 1977; Stöffler et al., 2013). The crater's present morphology is characterized by a fairly circular and relatively flat inner basin (Pohl et al., 1977). The impactor is thought to be a ~1.5 km-diameter asteroid that hit the surface with a velocity of ~20 km/s and generated a peak pressure of 100 GPa (Stöffler et al., 2002). The target rocks consist of ~600 m thick Triassic, Jurassic, and Tertiary sediments underlain by ca. 400-300 Ma crystalline basement. The latter is mostly gneiss and amphibolite with some granite (Pohl et al., 1977; Stöffler et al., 2013).

U/Pb dating of zircons from tuff beds over- and underlying the ejecta of the Ries impact and correspondence with the geomagnetic polarity time scale led Rocholl et al. (2018) to propose an age of the impact between 14.93 and 15.00 Ma corresponding to reversed polarity chron C5Bn1r. High precision $^{40}Ar/^{39}Ar$ dating of two tektites (glass produced from the Ries impact, called moldavite) by Di Vincenzo (2022) yielded 14.7495 ± 0.0045 and 14.7486 ± 0.0039 Ma, consistent with reverse polarity chron C5ADr. That paleomagnetic studies have ubiquitously identified reverse polarity in all impact-related melts (Koch et al., 2012; Pohl, 1965) dictates that the radiometric age corresponds to a reversed chron in the geomagnetic polarity reference timescale, meaning that the dates from Rocholl et al. (2018) and Di Vincenzo (2022) best match this criterion, with the latter having higher precision.

The Ries structure is characterized by well-preserved impact ejecta layers comprising Bunte Trümmermassen and suevite (Figure 1a). Bunte Trümmermassen includes Bunte Breccia and allochthonous sedimentary and crystalline basement megablocks, originating in the transient cavity. Because of the dominance of megablocks, the area between the inner ring and the structural ring is referred to as the megablock zone. Near the structural rim, this zone comprises parautochthonous megablocks of the target rock (Hüttner & Schmidt-Kaler, 1999).

Suevite is a polymict breccia of clastic material derived predominantly from the crystalline basement (e.g., von Engelhardt et al., 1969; Pohl et al., 1977; Stöffler et al., 2013). Suevite crops out as isolated patches on the inner ring, in the megablock zone, and reaches as far as ca. 23 km outside the rim. Suevite also occurs within the inner ring up to 300 m in thickness, deposited below post-impact lake sediments that can reach up to ca. 300 m in thickness (Pohl et al., 1977; Von Engelhardt, 1972). Suevite contains rock fragments that experienced all stages of shock metamorphism, as well as glass from the molten bedrock (Osinski et al., 2011; Stöffler et al., 2013). Temperature conditions during deposition were higher than 580°C, the Curie temperature of magnetite, because the suevite possesses thermoremanent magnetizations carried by magnetite that record a highly uniform direction and paleofield intensity throughout the crater (Koch et al., 2012; Pohl, 1965). The reversed polarity remanence directions produce negative magnetic anomalies in today's normal polarity magnetic field (Pohl et al., 2010).

The Bunte Breccia contains clastic material derived predominantly from the sedimentary cover that exhibits low shock stages ($P < 10$ GPa) with no evidence for melting; it is believed that the Bunte Breccia was heated to less than 100°C (Hörz & Banholzer, 1980; Von Engelhardt, 1990). Bunte Breccia deposits extend radially up to 45 km
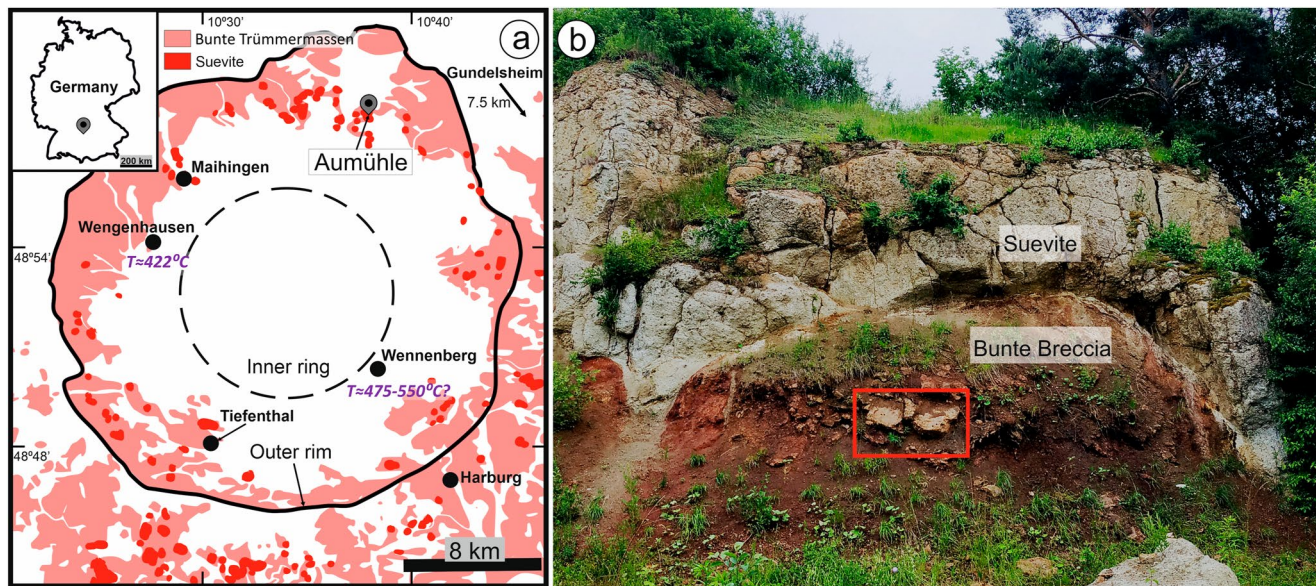
Figure 1. (a) Simplified geological map of Ries impactites depicting Bunte Trümmermassen and parautochthonous megablocks in pink and suevite in red (modified after Hüttner & Schmidt-Kaler, 1999). Black points indicate localities where basement rocks were collected; maximum impact heating temperatures are indicated in purple where constrained in this study. (b) Field photo at the Aumühle quarry showing the contact between suevite and Bunte Breccia. The image is roughly 8 m across. The red rectangle indicates limestone clast CB20 shown in Figure 2b.

from the center (Gall et al., 1975; Hüttner, 1969)—they comprise >90%/volume of the impact-related deposits outside the crater rim (Hörz et al., 1983). The Bunte Breccia was ejected ballistically, resulting in secondary cratering and an ensuing turbulent debris surge (Hörz et al., 1983; Oberbeck, 1975). Breccia derived from basement material is known as polymict crystalline breccia, where basement clasts of diverse lithologies can show evidence of shock conditions up to a few tens of GPa (e.g., Abadian, 1972; Von Engelhardt & Graup, 1984; Von Engelhardt, 1990; Hüttner & Schmidt-Kaler, 1999; Stöffler et al., 2013).

The Aumühle quarry (48°58′16.0″N, 10°37′47.6″E) possesses well-exposed outcrops spanning the contact between the Bunte Breccia and overlying suevite (Figures 1, 2 and 8). Just below the contact lies a poorly consolidated zone, which includes sedimentary and crystalline basement clasts. As such, this basement clast-rich horizon directly underlying the suevite might be termed polymict crystalline breccia, yet because abundant sedimentary clasts are present, and for the sake of simplicity, we refer to it as Bunte Breccia. The lowest part of the suevite is red, then turns gray within a stratigraphic thickness of 2–15 cm (Figure 2c); the suevite contains numerous vertical degassing pipes (e.g., Pietrek & Kenkmann, 2016). To better understand the formation conditions of the Bunte Breccia and the emplacement relationship with the suevite, we undertook a rock and paleomagnetic study supplemented by optical and scanning electron microscopy.

Using a battery-powered drill, we collected one to three, one-inch-diameter cores in 24 clasts (10 sedimentary and 14 basement clasts: CB01-CB24) in the Bunte Breccia, as well as two clasts in the suevite overlying the Bunte Breccia (CS01-CS02; Table S1 in Supporting Information S1). The clasts range from 5 cm to 1 m long and lie within 100 cm from the contact except for the largest clast (1 m long- CB20, Figure 2b), which lies about two m from the contact. We also drilled 54 cores in the suevite starting from the basal contact with the Bunte Breccia, where the suevite is red. About 12 cm above the first core, the color changes abruptly to gray, and we continued sampling until ~1 m above the transition. Of the two basement clasts drilled in the suevite, CS01 was taken right at the contact between the Bunte Breccia and the suevite, while CS02 was drilled 1 m above the contact. Cores were oriented using magnetic and, whenever possible, sun compass measurements. The average measured magnetic declination anomaly of 2.3 ± 1.2° ($N = 50$) conforms with that predicted by the international geomagnetic reference field (3.4°) for 2020.

In order to compare the magnetizations of the Bunte Breccia clasts with rocks of comparable lithologies, we collected 114 oriented cores from four basement blocks and two autochthonous limestone outcrops throughout the impact structure (Figure 1a): 14 Jurassic limestone cores from the Gundelsheim quarry (48°54′27.0″N, 10°49′49.3″E) where the strata are flat lying with striations oriented radially from the center of the crater; 10 limestone cores from Harburg (48°47′31.3″N, 10°41′50.1″E) southeast of the crater; 19 amphibolite cores from
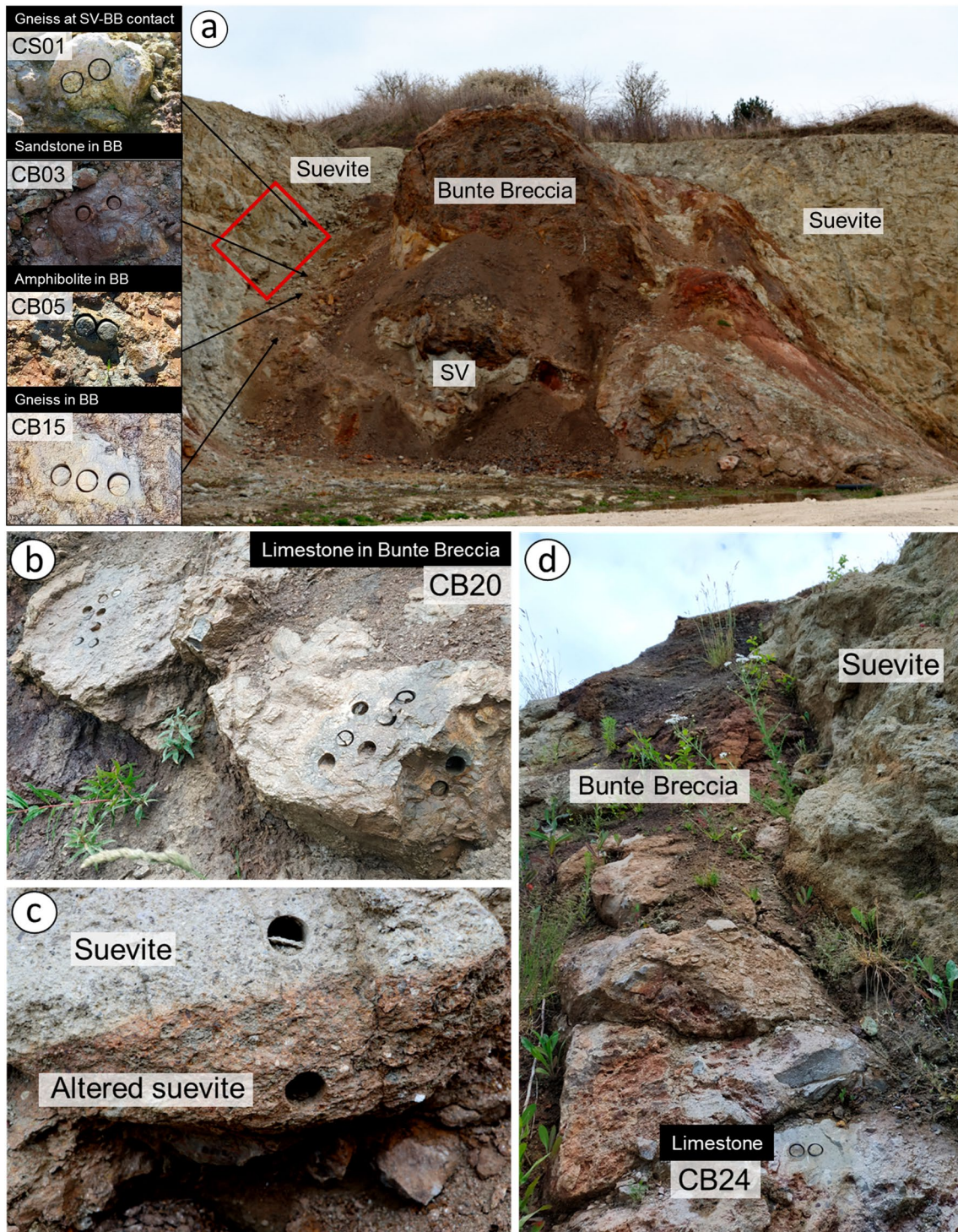
Figure 2. (a) View of Aumühle quarry outcrop showing complex relief of Bunte Breccia (BB) and suevite (SV). Oriented cores from 19 clasts were sampled from the top of the BB (four examples shown on the left). The red rectangle indicates the approximate location of Figure 8h. (b) A one-m-long limestone clast (CB20) in the Bunte Breccia was sampled ca. 40 m from the outcrop shown in (a). (c) Contact between gray and red (altered) suevite. (d) Outcrop of massive limestone near the contact between Bunte Breccia and suevite.

three limited outcrops distributed over ca. 100 m² near Tiefenthal (48°48′10.3″N, 10°29′51.7″E); six altered granitoid cores from Wengenhausen (48°54′40.0″N, 10°27′45.0″E); 30 cores of altered and somewhat brecciated granodiorite from Wennenberg (48°51′08.2″N, 10°37′44.5″E) near the inner crater ring (e.g., Stöffler

et al., 2013); and lastly 35 weakly shocked granite and gneiss cores from five outcrops distributed over a ca. 600 m² area around Maihingen (Klosterberg/Langenmühle: 48°56′02.1″N, 10°29′13.0″E). The basement rocks at Wengenhausen are overlain by shallow water carbonates deposited in the crater lake.

3. Experimental Methods

3.1. Rock and Paleomagnetism

Stepwise demagnetization experiments were performed on cylindrical specimens, 2.5 cm in diameter and 2.2 cm in height, at Ludwig-Maximilians-Universität (LMU, University of Munich) in a magnetically shielded room (~500 nT). Thermal demagnetization was done with an ASC Scientific TD-48 oven or a homemade oven (Volk, 2016) using 12 to 24 temperature steps from 25 to 680°C. Alternating field (AF) demagnetization up to peak fields of 90 mT was carried out using the automated SushiBar system (Wack & Gilder, 2012), which houses a three-axis, 2G Enterprises Inc., superconducting magnetometer to measure remanent magnetizations. Low-field susceptibility was measured with a Bartington Instruments MS2B sensor after each temperature step for a few samples per unit to monitor potential changes in magnetic mineralogy. Remanent magnetization directions were determined with principal component analysis (Kirschvink, 1980); mean directions were calculated using Fisher statistics (Fisher, 1953).

Hysteresis loops and backfield isothermal remanent magnetization curves were measured with a Lakeshore MicroMag 3900 vibrating sample magnetometer (5 mm-diameter cylinders). Thermomagnetic curves to estimate Curie temperatures were obtained with a Petersen Instruments variable field translation balance (5 mm-diameter cylinders). We also thermally demagnetized laboratory-induced isothermal remanent magnetizations (IRMs) imparted from three orthogonal fields of 1.0 T, 0.3 T, and 0.1 T (Lowrie, 1990) (2.5 cm-diameter cylinders) on the z, y, and x-axes of the samples, respectively. IRMs were measured with an AGICO JR-6 spinner magnetometer.

Partial thermal remanent magnetization (pTRM) experiments were carried out on six samples (5 mm-diameter cylinders) by imparting an artificial pTRM from 300°C to room temperature in an applied magnetic field of 50 µT along the samples' z-axes (I = −90°) followed by thermal stepwise demagnetization in four steps up to 400°C. Natural remanent magnetizations (NRMs) and laboratory TRMs of samples CB08_1, CB10_1, and CB16_1 were measured with an AGICO JR-6 spinner magnetometer, whereas NRMs and laboratory TRMs of samples CB01_1, CB09_2, and CB11_2 were measured with a 2G Enterprises Inc. superconducting magnetometer.

3.2. Microscopy

Polished and uncovered thin sections (25 µm) were made from 22 paleomagnetic cores (15 cores from Bunte Breccia clasts, 2 cores from suevite clasts, and 5 cores from suevite) and samples from Wengenhausen (CT913) and Wennenberg (CT1014) and investigated by polarization microscopy (Leica DM2700 P) using both reflected and transmitted light. Photomicrographs were taken with a Leica MC170 HD camera and processed with the Leica Application Suite X 3.08.19082 software. In situ micro-Raman spectroscopy was conducted to identify the Fe-bearing phases with a HORIBA Jobin Yvon XploRa ONE system at the Munich Mineralogical State Collection Munich (SNSB) (see Dellefant et al., 2023 for details).

Four clasts (CB05, CB09, CB20, and CS01), and two suevite samples (RS08, FD14) were studied with a Hitachi SU5000 scanning electron microscope (SEM) equipped with a backscattered electron (BSE) detector, energy-dispersive X-ray spectroscopy (EDS) detector (Oxford Instruments), NordlysNano high-sensitivity EBSD detector (Oxford Instruments), and a field emission gun. Chemical compositions were acquired with AZtec analysis software 4.2 (Oxford Instruments). SEM observations used working distances of 10 mm and accelerating voltages of 20 kV.

4. Results

4.1. Stepwise Demagnetization

4.1.1. Clasts in Bunte Breccia

Figure 3 shows orthogonal projections and normalized magnetization decay plots of five sedimentary and five basement clasts from the Bunte Breccia. For five clasts, one sample was subject to AF demagnetization and one to thermal demagnetization; demagnetization behavior varies highly among clasts, with a marked difference between sedimentary versus basement lithologies (Table S1 in Supporting Information S1). For 11 of 56 samples, stepwise demagnetization isolates a north and down direction at low AF fields (usually
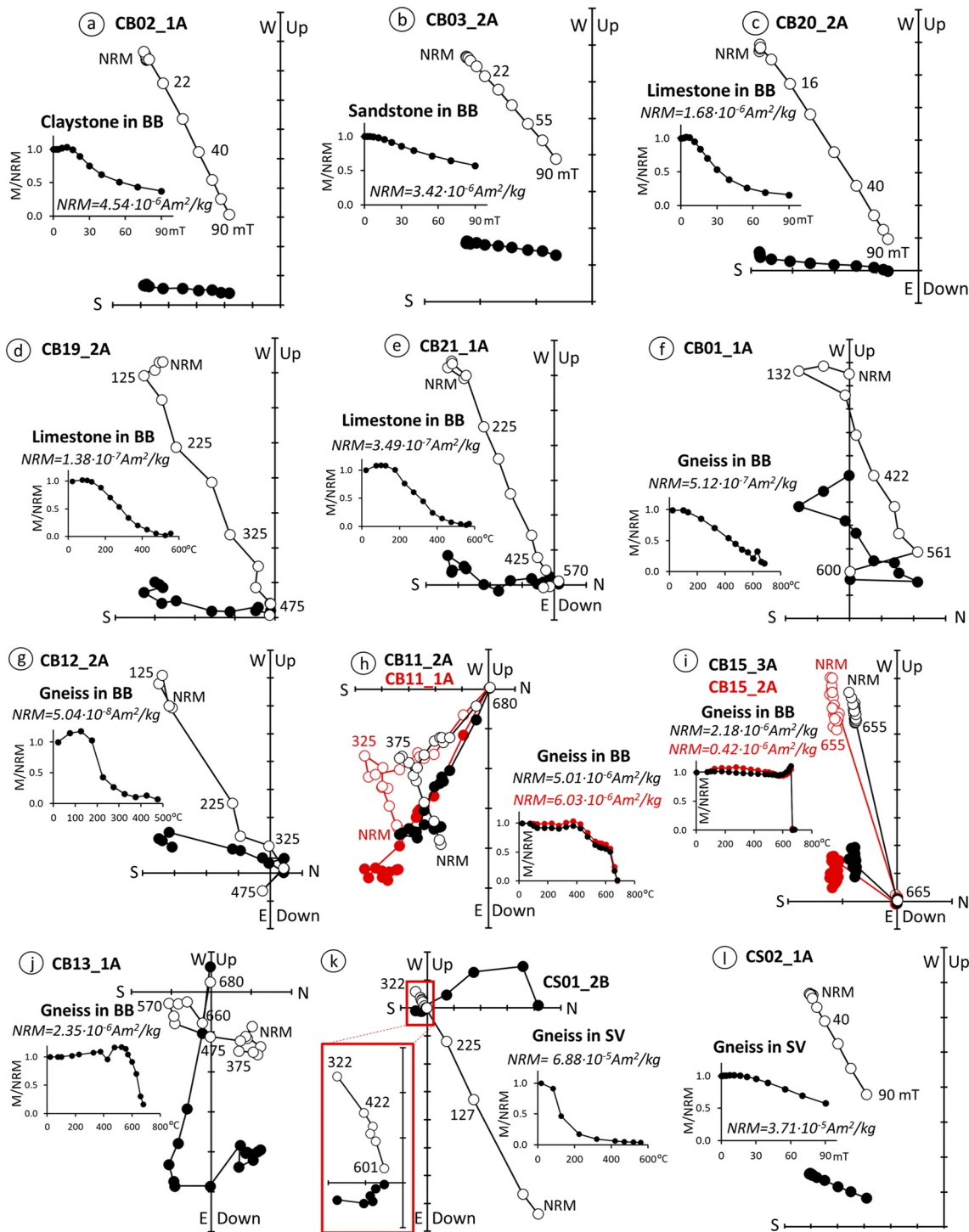
Figure 3. Orthogonal projections of stepwise demagnetization and normalized magnetization decay plots for clasts in Bunte Breccia (CB, BB) and suevite (CS, SV). Open (solid) circles on orthogonal diagrams denote the projection on the vertical (horizontal) plane; all plots in geographic coordinates. (a–e) Sedimentary clasts in Bunte Breccia; (f–j) basement clasts in Bunte Breccia; (k, l) basement clasts in suevite.

<15 mT, yet up to 40 mT) or below 275°C, with declination (D) = 1.3°, inclination (I) = 61.1° [radius of uncertainty at 95% confidence limits (α_{95}) = 6.0°], which is indistinguishable from the expected present-day geomagnetic field (D = 3.6°, I = 64.9°) at Aumühle (Figure 4a). We ascribe this component to a viscous overprint.
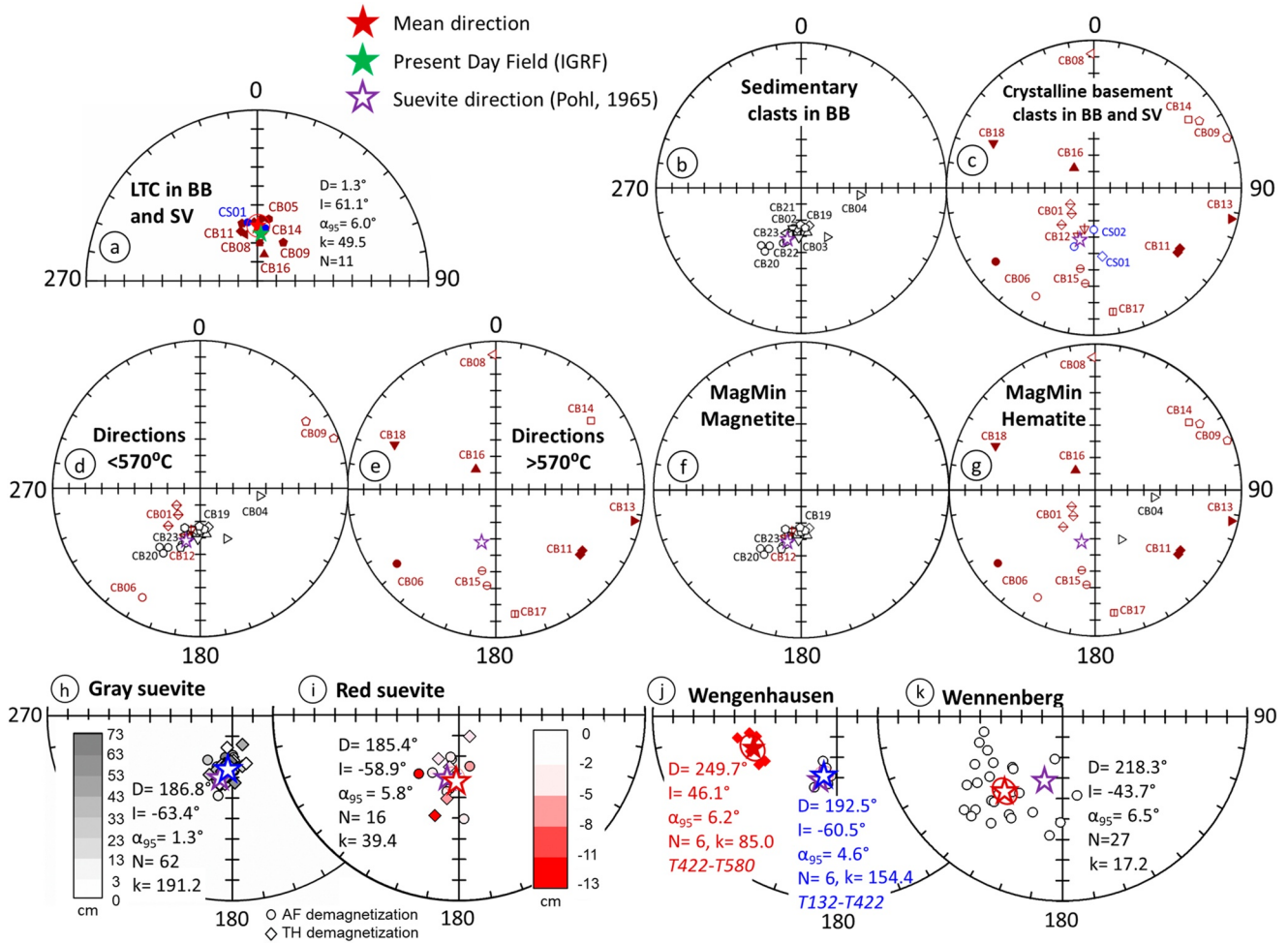
Figure 4. Stereographic projection of (a) low-temperature magnetization directions of clasts in Bunte Breccia. IGRF direction shown in green; (b) magnetization directions of sedimentary clasts in the Bunte Breccia, (c) magnetization directions of basement clasts in the Bunte Breccia (BB, in red) and in suevite (SV, in blue); (d) directions isolated below 570°C, (e) directions isolated from >570 to ~680°C; (f) magnetization directions of magnetite-dominated clasts in Bunte Breccia, (g) magnetization directions of hematite-dominated clasts in Bunte Breccia; (h) magnetization directions of all gray suevite samples color-coded by height, (i) of red suevite color-coded by depth (see Figure 8); (j) magnetization directions from Wengenhausen, and (k) from Wennenberg. Solid symbols plotted on the lower hemisphere, and open symbols are on the upper hemisphere. Mean directions and 95% confidence ellipsoids shown in red or blue, suevite direction acquired during the Ries event shown in violet.

For sedimentary clasts except for CB07, AF demagnetization removed 50%–80% of the original NRM by 90 mT defining directions with southward declinations and upward (ca. −60°) inclinations with linear demagnetization trajectories that may or may not decay to the origin on orthogonal diagrams (Figures 3a–3c, 4b). AF demagnetization was ineffective for most clasts from basement lithologies, removing only ≤10% of the NRM. For both sedimentary and basement clasts, thermal demagnetization below 580°C often isolated linear demagnetization trajectories with southward declinations and upward inclinations that did or did not trend to the origin (Figures 3d–3g, 4d). Directions typically became erratic in these samples above 580°C, like the hybrid case of CB01_1A in Figure 3f, where AF was ineffective. Basement clasts often had reproducible demagnetization trajectories when multiple cores were collected from the same clast (Figures 3h and 3i) with one or more demagnetization components. These samples fully demagnetized around 650–680°C, suggestive of (titano-)hematite. Samples that demagnetized in the titanohematite range had well-defined yet heterogeneous directions (Figures 3h–3j, 4e).

4.1.2. Clasts in Suevite

Demagnetization directions in two gneiss clasts within the suevite remained stable until ~570°C. Clast CS01 from the contact between the Bunte Breccia and the suevite had a strong recent field overprint at lower temperatures or AF fields (Figure 3k). Clast CS02 had very stable remanence upon progressive AF demagnetization
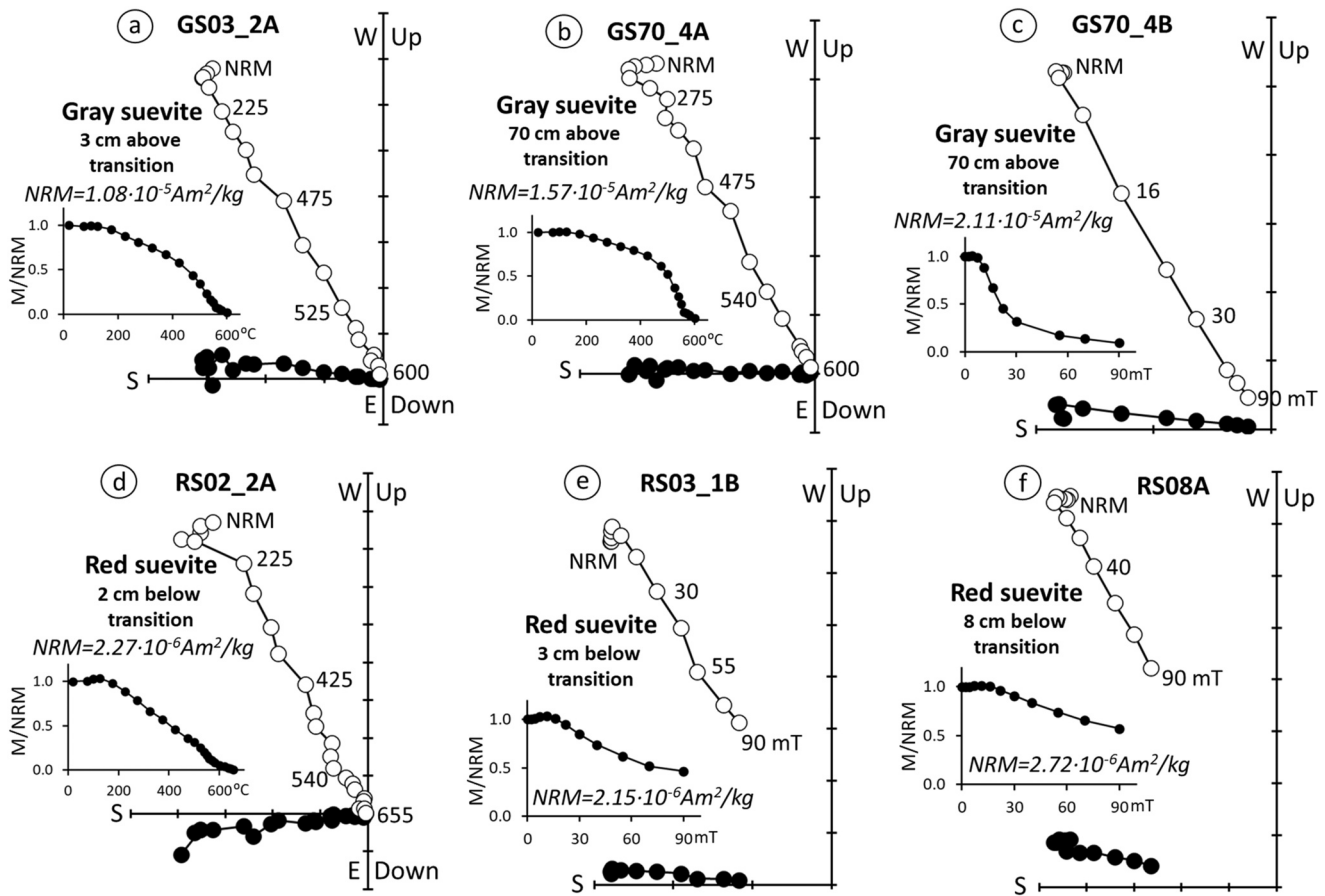
Figure 5. Orthogonal projections of stepwise demagnetization and normalized magnetization decay plots of (a–c) gray and (d–f) red suevite. Open (solid) circles on orthogonal diagrams denote the projection on the vertical (horizontal) plane; all plots in geographic coordinates.

with south and up-trending directions (Figures 3l and 4c). Neither of these two clasts had stable magnetization components above 570°C as opposed to the clasts in the Bunte Breccia.

4.1.3. Samples Collected Through the Red to Gray Suevite Contact

The basal part of the suevite grades from red to gray (Figures 2c and 8h). Using the red-gray transition as the baseline horizon (0 m), we collected 40 oriented cores (GS03–GS72) above the transition (positive values) until 72 cm and 14 oriented cores (RS02–RS12) up to −12 cm below the transition (negative values). The samples were drilled in a few stratigraphic profiles over a ca. 3 m wide surface.

Gray suevite samples ubiquitously display one dominant magnetization component unblocked by AF or thermal demagnetization with declinations of ca. 185° and inclinations of ca. −63° (Figures 5a–5c). Not forcing to the origin, with few exceptions, we fit the 22–90 mT steps and 425–570°C steps to define the characteristic components of 62 samples (for 8 out of 54 cores, two samples from a single core were used), yielding a mean of $D = 186.8°$, $I = −63.4°$ ($\alpha_{95} = 1.3°$, the Fisher (1953) precision parameter, $k = 191.2$) (Figure 4h). The overall mean direction defined by AF demagnetization ($D = 187.8°$, $I = −63.4°$, $\alpha_{95} = 2.1°$, $N = 28$) is indistinguishable at 95% confidence limits from that defined by thermal demagnetization ($D = 186.0°$, $I = −63.3°$, $\alpha_{95} = 1.7°$, $N = 34$) (Figure 4h). Gray suevite samples ($N = 15$) located within 15 cm from the contact have indistinguishable directions from 14 samples located 53–72 cm away from the contact, suggesting that the suevite cooled fast enough as not to record secular variation of the geomagnetic field in the time it took to cool through the blocking temperature of magnetite.

Red and gray suevite both display one dominant demagnetization component (Figures 5d–5f). Except for four samples farthest from the contact and closest to the Bunte Breccia, the characteristic magnetization component trends south and up: $D = 185.4°$, $I = −58.9°$ ($\alpha_{95} = 5.8°$, $k = 39.4$) (Figure 4i). A few characteristics distinguish

the red from the gray suevite. For one, the directions of the red suevite exhibit more dispersion than the gray suevite (compare Figures 4h and 4i). For another, AF is less effective at removing the NRM, and the magnetization directions defined by thermal demagnetization, albeit low in intensity, remain stable above 600°, whereas the gray suevite is fully unblocked by 580°C.

4.1.4. Samples Collected Outside of Aumühle

Thermal demagnetization of the Gundelsheim and Harburg limestones and the Maihingen granite and gneiss yielded noisy, uninterpretable demagnetization data (Figures 6a and 6b), with weak NRM intensities ($4.7 \times 10^{-8} \pm 2.5 \times 10^{-7}$ Am^2/kg). Conversely, the six samples from Wengenhausen displayed two consistent magnetization components (Figures 6c and 6d): one oriented south and up between 132 and 422°C ($D = 192.5°$, $I = -60.5°$, $\alpha_{95} = 4.6°$; Figure 4j) that did not trend toward the origin on orthogonal plots, and another oriented ca. $D = 249.7$, $I = 46.1°$ ($\alpha_{95} = 6.2°$; Figure 4j) that decays toward the origin by ca. 580°C. Demagnetization spectra of the Tiefenthal amphibolites varied widely from sample to sample with no coherent magnetization component. Both NRM ($2.8 \times 10^{-7} \pm 2.0 \times 10^{-5}$ Am^2/kg) and IRM ($7.2 \times 10^{-4} \pm 2.1 \times 10^{-2}$ Am^2/kg) intensities vary over three orders of magnitude, reflecting extreme heterogeneity in magnetic mineral concentration of the samples. In some cases, AF demagnetization removed more than 90% of the NRM, yet less than 10%–30% in others (Figure 6e). Thermal demagnetization likewise yielded a dichotomy of directions, none very coherent from one sample to the next (Figures 6f and 6g), although a south and down component can be vaguely extracted from most samples, but rarely in the same unblocking temperature or coercivity range. Most ($n = 27$ of 33) of the granodiorite samples from Wennenberg yielded a magnetization component with south-to-southwesterly declinations and upward-pointing inclinations unblocked by AF demagnetization above 7–11 mT and thermal demagnetization between ca. 225 and 475°C whose trajectories did not decay to the origin (Figures 6h and 6i). Above 475–570°C, the magnetizations become unstable. Best fit lines define a mean direction of $D = 218.3°$, $I = -43.7°$ ($k = 17.2$, $\alpha_{95} = 6.5$, Figure 4k), which is similar to the mean NRM direction ($D = 215.5°$, $I = -39.5°$, $k = 7.4$, $\alpha_{95} = 9.9$, $n = 33$). Both NRM ($2.1 \times 10^{-7} \pm 2.2 \times 10^{-7}$ Am^2/kg) and IRM ($1.2 \times 10^{-4} \pm 0.8 \times 10^{-4}$ Am^2/kg) intensities are quite constant among the 33 samples, reflecting relatively homogeneous magnetic concentrations.

4.2. Rock Magnetism

4.2.1. Clasts

Magnetic properties are highly variable among the gneiss clasts in the Bunte Breccia in concert with the results from thermal demagnetization (Table S1 in Supporting Information S1). Thermomagnetic curves are often noisy due to weak signals, although several are diagnostic of hematite. The common presence of more than one magnetic phase is indicated by wasp-waisted hysteresis loops and multiple inflections in the backfield curves (Figures 7a–7c; see also CB13 and CB15 in Figures S1a–S1f in Supporting Information S1). The slope of the thermomagnetic curve for CB10 flattens at 640°C, whose hysteresis loop seems to saturate, and the backfield curve reaches a stable plateau (Figures 7d–7f). CB16 has two very well-defined deflections at 340 and 580°C (Figure S1g in Supporting Information S1). Amphibolite clast CB05 has three Curie temperatures at ca. 150°, 340–360°, and 560–580°C (Figure S1j in Supporting Information S1). Hysteresis loops for these samples saturate and are rich in single-domain material based on the high remanence ratios (~0.30–0.44) and high coercivities of remanence (75–85 mT) (Figure S1 in Supporting Information S1).

Rock magnetic data of the sedimentary clasts in the Bunte Breccia are mostly consistent with the demagnetization data. Thermomagnetic curves were uninterpretable due to weak signals; however, three-component Lowrie demagnetization data were more revealing. The z-axis (1 T) curves often decay at 680°C, consistent with hematite, while the x- and y-axes have inflections at 580° (magnetite), 425°C (?), and around 325°C (pyrrhotite?) (Figures 7g–7i). Carbonate clasts CB19 and CB20 have deflections above 620°C yet below 680°C for the 1 T component and Curie temperatures of the medium (0.3 T) and low (0.1 T) fields at 580–620°C (Figure 7j). Hysteresis loops are not saturated by 1 T (Figure 7k). A significant difference for CB20 is that hematite appears as an important magnetic component in the rock magnetic experiments yet does not play an essential role as a remanence carrier, where >70% of the NRM is removed by AF demagnetization at 90 mT and >90% is removed below 580°C.

The thermomagnetic curve of gneiss clast CS01 at the contact between suevite and Bunte Breccia shows two major deflections around 300–350 and 560°C and lower magnetization during cooling, suggestive of the transformation of maghemite to hematite (Figure 7o). Lowrie demagnetization curves of gneiss clast CS02 entrained in the suevite reveal a minor presence of hematite (Figure 7n), whereas no trace of hematite occurs in limestone clast
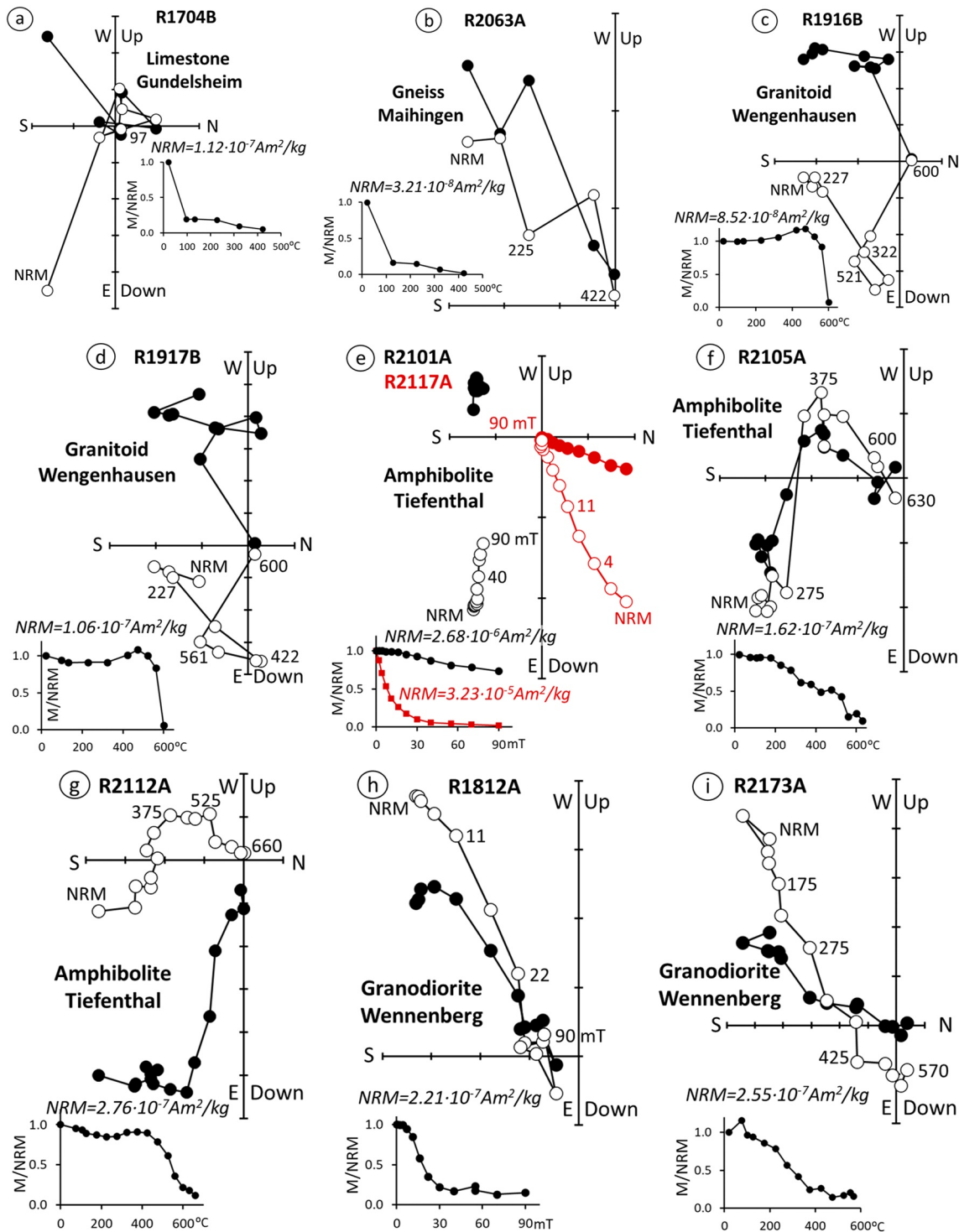
Figure 6. Orthogonal projections of stepwise demagnetization and normalized magnetization decay plots for basement rocks outside of Aumühle: (a) Gundelsheim limestone, (b) Maihingen granite and gneiss, (c), (d) Wengenhausen granitoid, (e)–(g) Tiefenthal amphibolite (magnetizations normalized in the orthogonal projections), and (h), (i) Wennenberg granodiorite. Open (solid) circles on orthogonal diagrams denote the projection on the vertical (horizontal) plane; all plots in geographic coordinates.
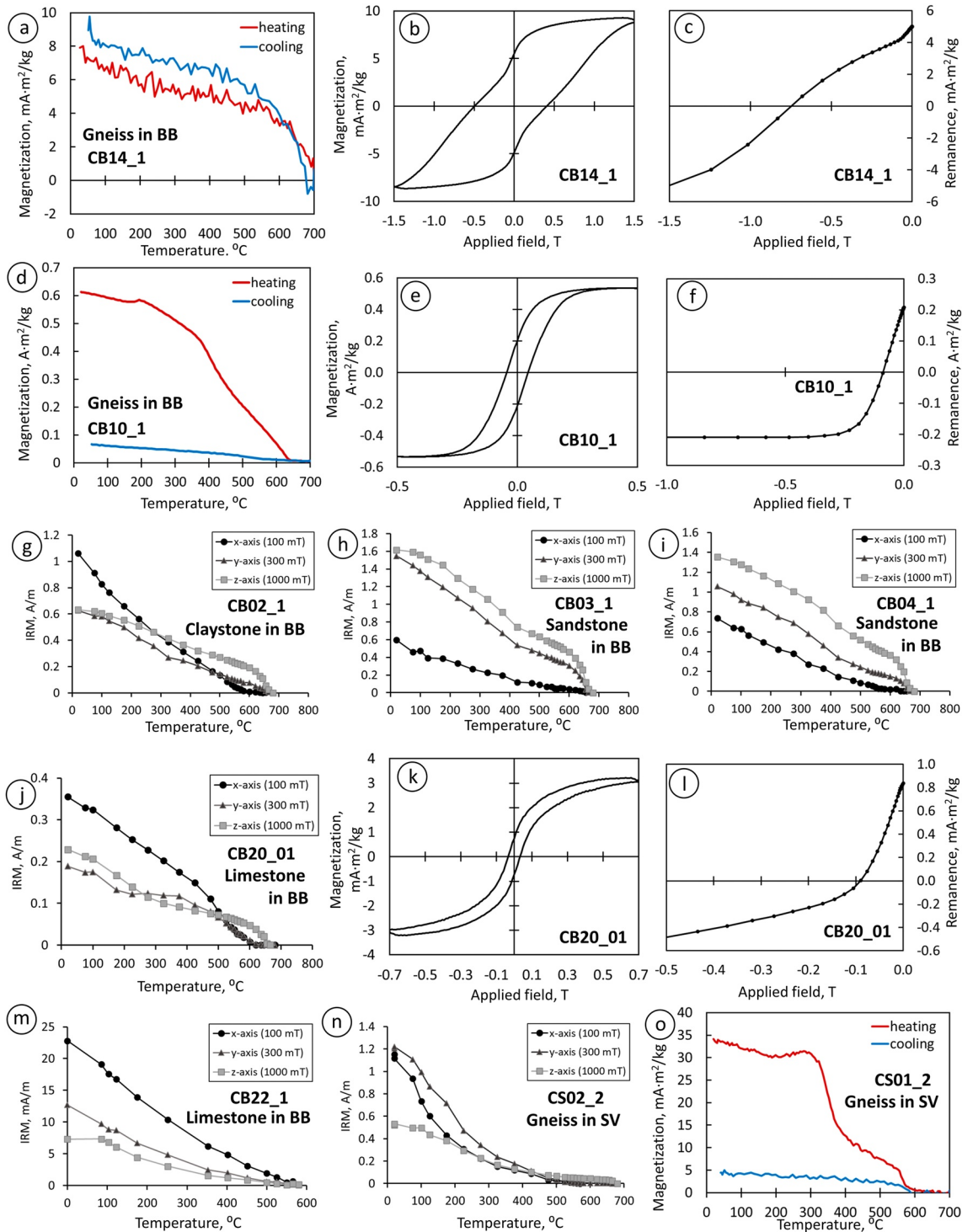
Figure 7. Rock magnetic experimental results from clasts in Bunte Breccia (CB, BB) and suevite (CS, SV). Thermomagnetic curves, hysteresis loops, and backfield curves for samples (a–c) CB14_1 and (d–f) CB10_1; Three-component IRM thermal stepwise demagnetization (Lowrie, 1990) curves for samples (g) CB02_1, (h) CB03_1, (i) CB04_1, and (j) CB20_01; (k) hysteresis loop and (l) backfield curve for sample CB20_01; three-component IRM thermal stepwise demagnetization curves for samples (m) CB22_1 and (n) CS02_2; (o) thermomagnetic curve for sample CS01_2.

Figure 8. Three-component IRM thermal stepwise demagnetization, hysteresis loops, and backfield curves for gray suevite (a–c) sample GS03_1 and red suevite samples (d) RS10_1 and (e, f) RS03_1. (g) $M_{475°C}/M_{NRM}$ and M_{90mT}/M_{NRM} as a function of distance from the red/gray suevite contact at 0 m. Gray symbols represent suevite above the contact, red symbols below. 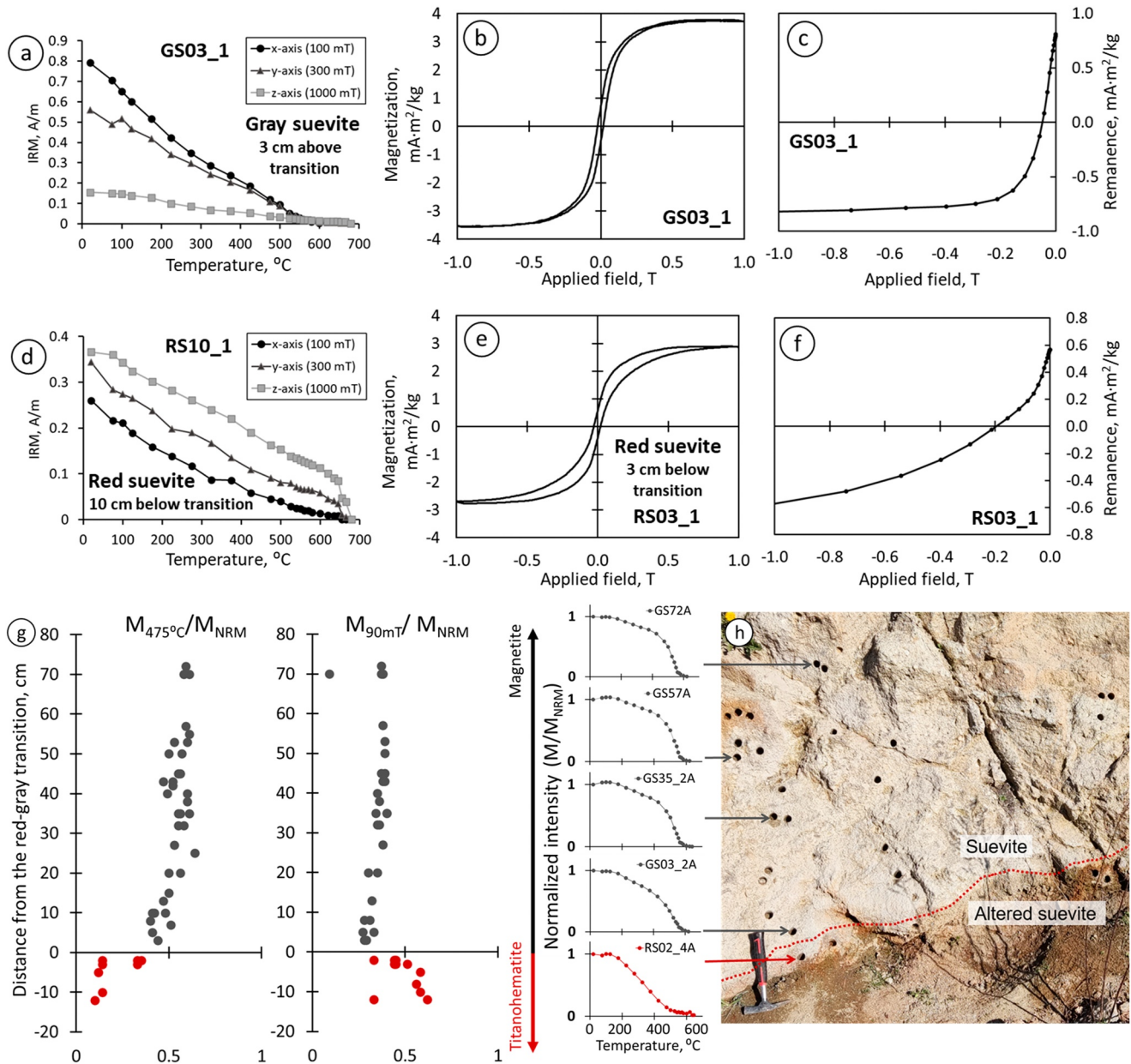(h) Photo of the suevite profile at Aumühle together with selected thermal decay plots of NRM; red dotted line indicates the red/gray contact.

CB22 (Figure 7m). A detailed microscopic investigation of CS02_1 (R20-16A) is given in Dellefant et al. (2023) who document magnetite formation coeval with impact.

4.2.2. Rock Magnetism of Suevite

Distinct differences in rock magnetic properties exist between the gray and red suevite: the NRM intensity of gray suevite is seven times higher ($1.7 \times 10^{-5} \pm 0.3 \times 10^{-5}$ Am^2/kg) on average than the NRM of red suevite ($2.5 \times 10^{-6} \pm 0.3 \times 10^{-6}$ Am^2/kg). Hysteresis loops are wasp-waisted for the red suevite (Figure 8e) and are not fully saturated by 1 T in contrast to gray suevite (Figure 8b). Lowrie demagnetization curves show significant inflections at ~580°C (Figure 8a) in the gray suevite, suggestive of magnetite, whereas the underlying red suevite exhibit inflections in higher temperatures around 640–680°C (Figure 8d), suggestive of Ti-free to Ti-poor titanohematite.

Figure 8g plots the $M_{475°C}/M_{NRM}$ and M_{90mT}/M_{NRM} ratios against distance from the red-gray transition as the baseline horizon (0 m), where $M_{475°C}$, M_{NRM}, and M_{90mT} are the magnetic moments after heating to 475°C, the NRM and after AF demagnetization to 90 mT, respectively. In the gray suevite, a slight decrease in $M_{475°C}/M_{NRM}$ is observed toward the contact between two types of suevite, while in the red suevite, this ratio sharply decreases immediately below the red-gray transition and becomes three times lower than in the gray suevite. M_{90mT}/M_{NRM} is relatively constant for the gray suevite, then suddenly increases below the red-gray transition.

4.2.3. Rock Magnetism of Sites Outside Aumühle Quarry

None of the exposed basement rocks exhibit remanent magnetization in the temperature range of hematite, although hysteresis and backfield data (Figure S5 in Supporting Information S1) indicate that Maihingen and Tiefenthal lithologies contain minerals with high coercivities. Rock magnetic characteristics between the basement clasts at Aumühle and the basement blocks around the impact structure are significantly different (Table S3 in Supporting Information S1). NRM/IRM values for the gneiss and limestone clasts in Bunte Breccia are 32–36 times larger than for rocks of similar lithologies outside Aumühle, suggesting a different nature of their NRMs.

4.3. Shock Effects in Bunte Breccia and Suevite Clasts

The clasts in the Bunte Breccia exhibit a wide variety of shock effects (Table S1 in Supporting Information S1). Below, we describe some key findings highlighting the shock levels in selected clasts together with the magnetic mineralogy.

4.3.1. Amphibolite Clast in Bunte Breccia

Amphibolite clast CB05 contains fractured and twinned amphibole and maskelynite, a diaplectic glass with a composition of feldspar (Figure 9a). Planar features within maskelynite exhibit extinction positions with crossed polarizers (Figure 9b), indicating optically anisotropic feldspar remnants. Magnetite ranges from 50 μm to mm in size (Figure 9c) and can contain μm-sized hematite exsolutions (Figure 9d), ~10 μm hematite laths, and/or an oxidation rim of hematite. Hematite may also occur as either ~40 μm-sized grains or as a fine-grained precipitate along fractures in amphibole, where fine-grained limonite can also occur. Shock effects indicate pressures of 20–34 GPa (Stöffler et al., 2018).

4.3.2. Gneiss Clasts in Bunte Breccia

Here, we briefly recap the main observations from gneiss clasts sampled in the Bunte Breccia. Clast CB01 contains >100 μm-sized, optically isotropic phases of feldspar composition (maskelynite), quartz with planar deformation features (PDFs), and biotite. Hematite occurs as individual, 10s of μm-sized grains or as finer grains dispersed within biotite. Sample CB06 contains 100 μm-to-mm sized quartz bands with PDFs and undulous extinction, as well as coarse feldspar and bands of phyllosilicates, such as biotite/chlorite and muscovite with fine-grained limonite. Hematite occurs as ~50 μm-sized grains and as fine-grained oxidation products within phyllosilicates. Sample CB14 contains >100 μm maskelynite, quartz displaying PDFs, and biotite; ~200 μm-sized magnetite occurs as individual grains or as bands within the rock fabric often oxidized to hematite, which can also be seen as fine-grained material on grain boundaries. Sample CB12 stems from a gneiss clast with a calcite vein and hundreds of μm-sized feldspar and biotite/chlorite grains, as well as quartz that rarely shows PDFs. Rutile grains (~40 μm) occur together with fine-grained hematite and limonite. Sample CB11 contains abundant μm-sized fractured feldspar and quartz grains with few observable PDFs. Hematite occurs as μm to 150 μm-sized grains together with ~70 μm-sized ilmenite with μm-scaled rutile exsolutions and vice versa. Sample CB09 shows hundreds of μm-sized quartz grains with PDFs and maskelynite as well as biotite/chlorite. Around 70 μm-sized grains consisting of a ~30 μm pyrite core rimed by μm-sized hematite occur together with ~50 μm-sized hematite grains with a fine-grained core (Figures S2a, S2b in Supporting Information S1). Shock effects indicate pressures up to 35 GPa (Stöffler et al., 2018).

4.3.3. Gneiss Clast at the Contact Between Bunte Breccia and Suevite

Sample CS01 has a foliation consisting of altered feldspar with layers of diaplectic SiO_2 in association with biotite. The diaplectic SiO_2 glass (Figures S2c, S2d in Supporting Information S1) shows broad Raman peaks approximately at 472, 603, and 821 cm^{-1} (Kowitz et al., 2013). Magnetite grains of ~300 μm are fractured and locally replaced by fine-grained hematite and anatase (Figures S2e, f in Supporting Information S1), where ilmenite laths can be locally observed. Rutile grains up to hundreds of μm occur with μm-scaled hematite exsolution features. Shock effects indicate pressures of 35–45 GPa (Stöffler et al., 2018).
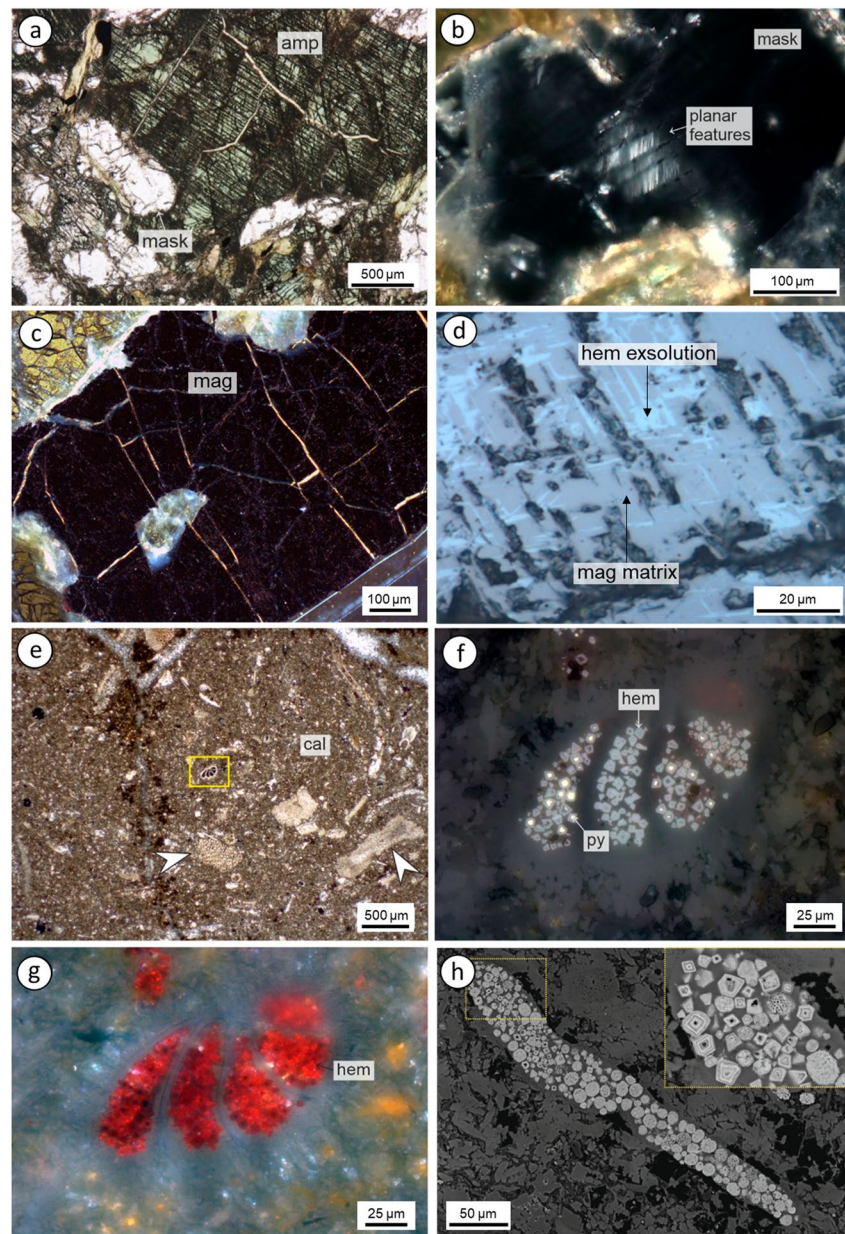
Figure 9. Micrographs of Bunte Breccia clasts. (a)–(d) Amphibolite clast CB05 showing (a) amphibole (amp) with planar elements and maskelynite (mask) observed in (a) transmitted single polarized light and (b) maskelynite (mask) and planar features in a residual plagioclase crystal, transmitted light and crossed polarizers. (c), (d) Magnetite (mag) containing μm-sized exsolutions of hematite (hem) (c) in transmitted light and crossed polarizers and (d) transmitted light and single plane polarization. (e) Fossil-rich (white arrows) limestone clast CB20 composed of fine-grained calcite matrix (cal) and framboids in the fossil remnants in transmitted single plane polarized light [yellow rectangle, magnified in (f) and (g)]. (f), (g) Framboids with pyrite (py) cores and hematite (hem) rims. Reflected light with (f) single plane polarization and (g) crossed polarizers. (h) BSE image of worm-like agglomeration of framboids.

4.3.4. Sedimentary Clasts in Bunte Breccia

The grain-supported and clay-cemented, well-sorted quartz sandstone (CB03) within the Bunte Breccia displays grain sizes ranging from 5 to 40 μm with no pore spaces; limonite occurs ∼5%, with rare hematite and anatase. The one-m-sized limestone clast (CB20) hosts several fossils (Figures 9e–9h) that contain framboids of euhedral, cubic, μm-sized aggregates consisting of pyrite in the core and fine-grained hematite at the rim. Raman analysis suggests that magnetite may have been generated from pyrite with a subsequent transformation to hematite. This

interpretation is based on the relatively strong occurrence of the magnetite main peak shift at about 660 cm^{-1} (Figure S2g in Supporting Information S1), as well as the magnetic data suggesting magnetite is the main carrier of the remanence, together with minor hematite. The limestone shows no apparent shock effects; 50–150 μm wide fractures are filled with calcite.

4.3.5. Suevite

The suevite in direct contact with the underlying Bunte Breccia (Figure S3a in Supporting Information S1) has ~40% of fine-grained matrix (Figure S3b in Supporting Information S1) composed of several μm-sized mineral and lithic components as well as glass fragments. Lithic clasts are up to dm-sized ~70% crystalline and ~20% sedimentary (quartz sandstone prevalent) rocks, with the rest being ~10% mineral components. Silicate mineral clasts range from 50 to 500 μm with an average of ~200 μm and can be identified as mostly quartz and feldspar with minor amounts of biotite and calcite (Figure S3b in Supporting Information S1). Quartz-rich clasts as well as quartz in lithic clasts contain PDFs. Glass fragments occur about 10% and range from 200 μm to 5 mm with a homogeneous distribution and spheroid to elongated shapes, often with an internal flow-structure and voids (Figures S3c, d in Supporting Information S1). Regimes within the glass fragments show a composition of almost pure SiO_2 (Figure S3c in Supporting Information S1). The altered suevite is characterized by a red color (samples RS12_1, RS08, FD14), which is attributed to fine-grained euhedral and zoned iron oxides and hydroxides, such as hematite and limonite, which occur along clast boundaries and within voids (Figures S3c, d in Supporting Information S1). Furthermore, ~100 μm-sized magnetite, ~40 μm-sized rutile, ~100 μm-sized anatase, and ~80 μm-sized sphene can occur.

5. Discussion

5.1. Magnetization Components in the Bunte Breccia

Remanent magnetization directions in the Bunte Breccia fall into two groups: (a) those whose directions are well clustered with southerly declinations (ca. 190°) and upward inclinations (ca. −60°) (Figures 4b, 4d, 4f) and (b) those with heterogeneous (random) directions (Figures 4c, 4e, 4g). The first group was mostly isolated by alternating field demagnetization from 20–50 to 90 mT or thermal demagnetization below the Curie temperature of magnetite (580°C). The second group was isolated by thermal demagnetization above 580°C, up to 680°C, suggestive of Ti-free to low Ti titanohematite; AF demagnetization to 90 mT typically only removed ca. 10% of the NRM. Rock magnetic experiments (Figure 7 and Figure S1 in Supporting Information S1) are mostly consistent with the interpretation of the demagnetization experiments (Figure 4). Paleomagnetic behavior varies according to clast lithology (Table S1 in Supporting Information S1), with almost all sedimentary clasts belonging to the first group, while most (10 out of 14) basement clasts belong to the second group. However, several exceptions exist (Figures 4d and 4e vs. Figures 4f and 4g). Two samples from sedimentary clast CB04 lost only 50% of their NRM after AF demagnetization to 90 mT. One has $D = 152.2°$ and the other $D = 97°$, both with I ~ −54° (Table S1 in Supporting Information S1); Lowrie experiments identify abundant hematite. Paleomagnetic directions in gneiss clasts CB01 and CB09 were fit in the magnetite unblocking range; the magnetization becomes unstable above 580°C, although rock magnetic experiments reveal the dominant presence of hematite (Table S1 in Supporting Information S1). Clast CB06 possesses two magnetization components and contains hematite.

Paleomagnetic directions from the first group (Figures 4b and 4d), referred to as the "Ries" component, conform to the directions in suevite throughout the Ries crater ($D = 194.4°$, I = −56.8°, $\alpha_{95} = 2.0°$ in Pohl (1965); $D = 194.4°$, I = −57.5°, $\alpha_{95} = 5.7°$ in Koch et al. (2012)). Directions from the second group are randomly oriented according to the Watson (1956) randomness test, which we refer to as the "Random" component. In the case of only clasts with directions isolated by thermal demagnetization above 580°C up to 680°C ($N = 11$, 5% significant point $R_0 = 5.29$), $R = 2.74$; after including clasts CB04, CB01, CB09, and CB06 ($N = 19$, $R_0 = 6.98$), then $R = 5.25$. Such differences between "Ries" and "Random" components raise the question of their origin, which should be due to thermal (thermal remanent magnetization, TRM: cooling of pre-existing magnetic minerals through the Curie temperature) and/or chemical (chemical remanent magnetization, CRM: chemical growth of new magnetic minerals through the blocking volume) processes, as explained below.

5.2. Origin of the Magnetization Components in the Bunte Breccia

Clasts carrying the Ries component have unblocking temperatures up to 580°C, which is the minimum temperature that the clasts should have been heated to, in order to acquire a TRM. In this scenario, the clasts would have been emplaced, then heated up to the Curie temperature of magnetite from the hot overlying suevite. They

could not have been heated above ∼640°C, otherwise, the clasts containing titanohematite would also carry the Ries component. Another way to acquire the Ries component is if chemical alteration in the sedimentary clasts produced magnetite and/or iron sulfide phases, which are commonly found in overprinted carbonate rocks; for example, compare Figures 4, 5 and 10 in Huang et al. (2017), Figures 2 and 3 in Sun and Jackson (1994), and Figures 11a–11d; 12a-c in Weil and Van der Voo (2002) with Figures 9h and 9f from the Ries carbonate clasts. Rocks possessing CRMs acquired at or soon after deposition would record the Ries direction. Since the CRM acquisition process depends on growing through the blocking volume (ca. 30 nm for magnetite and hematite; Dunlop & Özdemir, 1997) and not cooling through the blocking temperature (Néel, 1949), the temperature of the fluid/gas leading to a CRM can be well below the Curie temperature, even though the samples demagnetize up to the Curie temperature. Distinguishing TRM and CRM is challenging due to similarities in unblocking spectra (Draeger et al., 2006; Kobayashi, 1959).

It is more difficult to explain the origin of the Random component. We do not think the random orientations among the clasts is a recent phenomenon or sampling artifact due, for example, to quarrying of the section, gravity sliding, lightning, and so on, for the following reasons. First, when present, the low-temperature component parallels the present-day field direction (Figure 4a). Had the clasts rotated within the short time (< 1 month) between quarrying and sampling, the short time would necessitate a large proportion of superparamagnetic grains, which we found no evidence for, thereby suggesting the viscous component was acquired over time scales predating quarrying. Hence, those clasts were likely in place since cratering. Second, paleomagnetic directions of multiple cores drilled in the same clast are quite consistent (Figures 3h and 3i; Table S1 in Supporting Information S1), as are their NRM intensities, which argue against lightning strikes that would remagnetize the clasts over very local spatial scales (Carporzen et al., 2012). Third, it is difficult to imagine a scenario where clasts containing hematite were systematically rotated during or since quarrying of the section, but clasts with magnetite were not. In this light, the randomly oriented directions among the clasts must have a physical meaning intrinsic to the cratering process.

Hydrothermal fluids can alter pre-existing Fe-bearing phases in the clasts to titanohematite, both of which would acquire a CRM (Kim et al., 2009; Larson et al., 1982; Walker et al., 1981). That the basement rocks we studied outside the Aumühle quarry show no evidence of magnetic remanence in the hematite temperature range likely suggests that the hematization occurred during or after the impact, not before. However, the only plausible scenario requires that the clasts carrying the Random component acquired their remanences first, and then rotated about independent axes during or prior to deposition. This is consistent with the interpretations of Hörz et al. (1983) and Oberbeck (1975) who regarded the Bunte Breccia as a turbulent mixture resulting from ballistic deposition. They argued that the Bunte Breccia represents a chaotic environment that was emplaced in a brief period of approximately 5 minutes. Using a thermal diffusivity characteristic of gneiss (10^{-6} m²/s) and assuming conductive cooling proportional to the square of the sample radius, we estimate that a clast with a 10 cm radius would take several minutes to cool from 700°C (the assumed initial temperature) to 580°C. Therefore, if the clasts were turbulently deposited, they must have been deposited in an environment below the blocking temperature of titanohematite (ca. 640–680°C), otherwise, they would carry the Ries component.

If the depositional environment of the basement clasts was hot (≥300°C), we would expect to see a partial thermal overprint (pTRM) with the Ries direction in the low-temperature unblocking region followed by randomly oriented directions above. This would be the scenario to explain the two remanence components from Wengenhausen, discussed below. The ability to create a pTRM depends on Curie temperature and grain size—single-domain magnetite or hematite grains can be heated close to their Curie temperatures for millions to billions of years without spontaneously flipping their magnetic moments (Pullaiah et al., 1975). The high coercivities, hysteresis parameters, and unblocking spectra of the hematite-bearing basement clasts suggest the hematite is rich in single domain grains in some clasts (Figures 3i, 7a–7c), and if so, they should be expected to resist a pTRM with the Ries direction even if significantly heated for long time periods.

To investigate this possibility, we undertook an experiment on six samples by first measuring their NRMs and then imparted an artificial partial TRM from 300°C to room temperature in an applied magnetic field of 50 μT along the samples' z-axes (I = −90°). The laboratory TRM was measured and then thermally stepwise demagnetized in four steps to 400°C (Table S2; Figure S4 in Supporting Information S1). The results are quite striking—samples rich in magnetite acquired a TRM roughly parallel to the applied field, while those dominated by hematite did not (Figure S4 in Supporting Information S1). CB01_1 acquired a pTRM that does not decay to the origin which
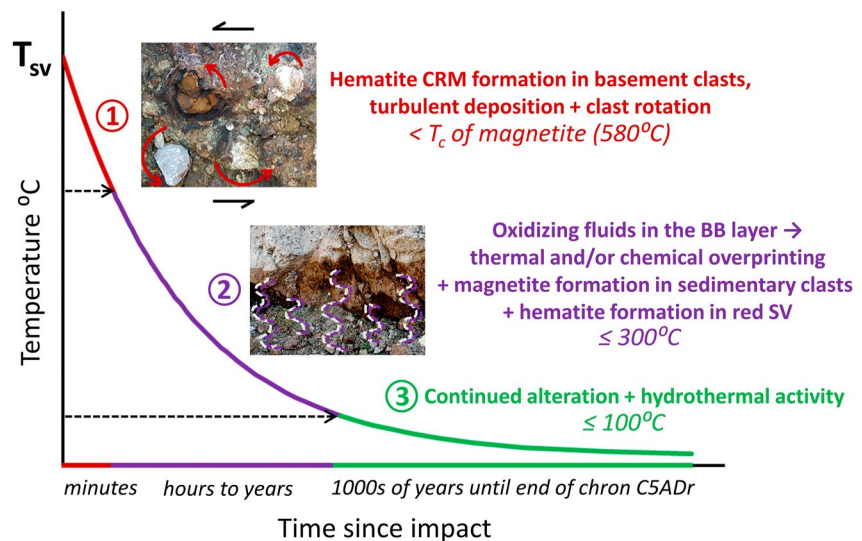
Figure 10. Thermal history of the Aumühle quarry divided into three phases. (1) Hematite grew, and remanence was blocked in the basement clasts, then the clasts rotated under turbulent deposition. The maximum temperature in this phase was the temperature of the suevite (T_{SV}). This phase ceased below the Curie temperature of magnetite as some magnetite-bearing clasts were also rotated. (2) After turbulent deposition ceased, oxidizing fluids in the Bunte Breccia (BB) layer continued to cause alteration and concomitant precipitation of magnetite and hematite, producing a CRM in, for example, the carbonate clasts and at the base of the suevite, whose magnetite was partially converted to hematite. (3) Low-temperature oxidation and hydrothermal activity continue up to thousands of years at most until the end of reversed chron C5ADr.

has I = −90° (Figure S4e in Supporting Information S1); however, the pTRM directions lie far from the applied field direction. This is consistent with the demagnetization of the original NRM of CB01_1, which yields the Ries direction below 561°C (Figure 3f). Moreover, after normalizing the TRM intensity by the laboratory field (50 µT) (TRM*) and normalizing the NRM intensity by the 15 Ma Ries paleofield (19.2 µT; Koch et al., 2012) (NRM*), TRM*/NRM* is close to 1 for magnetite-bearing clasts and around 0.3 for hematite-bearing clasts. These experiments demonstrate that, if heated to 300°C, clasts with significant amounts of magnetite are likely to acquire full or partial TRMs, while hematite-rich clasts will not.

5.3. Time-Temperature Evolution of the Bunte Breccia-Suevite Contact Zone at the Aumühle Quarry

The fact that basement blocks outside Aumühle do not contain stable, well-defined remanence directions above 580°C (Figure 6) means that the generation of hematite in the Bunte Breccia basement clasts occurred during or after the excavation process. Because the remanence directions are randomly oriented, the clasts must have acquired their remanences and were then reoriented (rotated) before final deposition. This is consistent with the irregular contact between the Bunte Breccia and suevite at Aumühle. Therefore, hematite growth and remanence acquisition in basement clasts happened between the time of impact and cessation of turbulent movement of the Bunte Breccia clasts after emplacement of the suevite, hence likely within seconds to minutes. The shock effects observed in the basement clasts from the top layer of Bunte Breccia indicate shock conditions up to 35 GPa and post-shock temperatures up to 300°C (Stöffler et al., 2018). We consider this as the first of three general phases that describe the emplacement of the Bunte Breccia and suevite at the Aumühle quarry (Figure 10).

Heat acting to chemically produce magnetite (or Fe sulfides) in the limestone clasts or further alteration to hematite, such as the conversion of gray into red suevite (Figure S4 in Supporting Information S1), must have occurred during reversed polarity chron C5ADr (Di Vincenzo, 2022), as all directions have reversed polarity. Chron C5ADr ended at 14.609 Ma (Ogg, 2020). Given the average age of 14.74805 Ma for the Ries crater means that the maximum duration for hydrothermal alteration was 139 kyr following crater formation. Temperatures were not high enough to reset the paleomagnetic directions in pre-existing hematite nor in the magnetite-bearing gneiss basement clasts with the Random component (CB06, CB09; Figure 4d). Those few magnetite-bearing basement clasts with the Random component must have held pre-existing remanences, then were rotated during turbulent deposition and not thermally reset. Hence, the temperature of the fluid-rich horizon in the Bunte Breccia zone was lower than the Curie temperature of magnetite (580°C).

How hot were the fluids in the Bunte Breccia layer? The presence of impact glass exhibiting flow fabrics in the suevite (Osinski, 2004) and the existence of decarbonated rims on limestone clasts (Baranyi, 1980) suggest initial deposition temperatures of 750–900°C. Ilmenite within suevite clast CS02 transformed to pseudorutile at temperatures <700°C (Dellefant et al., 2023). Studies on shock effects in the Bunte Breccia have indicated maximum temperatures of about 100°C (Hörz & Banholzer, 1980; Von Engelhardt, 1990); however, this concerns only the process occurring under shock conditions. Creation of a CRM depends on the reaction kinetics—the higher the temperature, the faster conversion will occur. We suspect that hematite formation in the basement clasts was accomplished very quickly (seconds to minutes) under hot ionizing conditions, whereas hematite growth at the base of the suevite and Bunte Breccia layer took place at lower temperatures under protracted time scales (tens to thousands of years).

In contrast to the basement clasts, the sedimentary clasts within Bunte Breccia show no apparent shock effects, consistent with previous studies claiming that the Bunte Breccia experienced low shock stages ($P < 10$ GPa) with no evidence for melting (Hörz & Banholzer, 1980; Von Engelhardt, 1990). Most of the sedimentary clasts in our study are limestones, where even at low shock pressure conditions undulatory extinction and calcite twinning would be expected (e.g., Kurosawa et al., 2022; Langenhorst et al., 2003; Seybold et al., 2023). In the studied limestone clasts, no indication of shock-induced undulatory extinction or twinning of calcite was observed. Aggregates of pyrite in the core rimmed by fine-grained hematite and magnetite are clearly of secondary origin. Raman spectra suggest magnetite could have been generated from pyrite with a subsequent partial transformation to hematite (Figure S2g in Supporting Information S1). These iron oxides and sulfides were formed in situ and possess the Ries component. As almost all the sedimentary clasts have the Ries component, we conclude that the CRMs formed at lower temperatures than the hematite hosting the Random CRM. The model in Figure 10 thus separates the two processes, placing the magnetite CRM later in time and lower in temperature than the hematite CRM. It is also possible that in some cases magnetite was further altered to hematite, as seen in clast CB20 and the red suevite. The pTRM experiments (Figure S4 in Supporting Information S1) suggest 300°C is sufficient to thermally overprint magnetite-bearing clasts with the Ries direction, however, it is difficult to know whether there are combined Ries components with both CRM and TRM.

According to rock magnetic data, the basal part of the suevite was partially chemically altered, as hematite precipitated along grain boundaries in the red suevite (Figure S3 in Supporting Information S1), likely due to the oxidation of magnetite to hematite, leading to the red color (Figure 8h). Although the average magnetization direction in the gray suevite ($D = 186.8°$, I = $−63.4°$, $\alpha_{95} = 1.3°$) is indistinguishable from the red suevite ($D = 187.9°$, I = $−57.8°$, $\alpha_{95} = 5.8°$) at 95% confidence limits (McFadden & Lowes, 1981), the scatter about the mean is much less in the gray suevite ($k = 191$, $N = 62$) than in the red suevite ($k = 39$, $N = 16$). Coercivity and unblocking temperature spectra of suevite indicate that its lower part is partially chemically altered to titanohematite, likely formed by hydrothermal activity under oxidizing conditions. Titanohematite content decreases upwards from the suevite-Bunte Breccia contact, with magnetite being dominant 12 cm above the contact. As the spontaneous magnetization of titanohematite is ca. 250 times less than magnetite (Dunlop & Özdemir, 1997), chemical processes reduced remanence intensity while directions remained unaffected. We think the much lower scatter (higher k) in the gray versus red suevite reflects differences in time of remanence acquisition, with the magnetite in the gray suevite cooling through the Curie temperature fairly instantaneously thereby not averaging secular variation, while the hematite formed over longer time to sufficiently average geomagnetic secular variation. According to Deenen et al. (2011) a k of 39 lies between the lower and upper limits of 12.5 and 50.0, which can be reasonably explained by paleosecular variation; $k = 191$ clearly does not average secular variation. Importantly, the observations suggest that the overlying suevite acted as a barrier with very low permeability that confined oxidizing fluids to the permeable Bunte Breccia zone, with only the lowermost suevite being altered by the fluids near the contact (Figure 10). Heap, Gilg, Byrne, et al. (2020) determined that the average permeability of suevite from Aumühle is $8.20 \times 10^{−15}$ m^2. Permeability data of suevite from other locations in Ries can be found in Parnell et al. (2010) and Heap, Gilg, Hess, et al. (2020).

High-temperature (~300°C) hydrothermal activity has been attributed to the crater suevite acting as the heat source (Muttik et al., 2010; Osinski, 2005). Localized low-temperature (~100°C) hydrothermal activity has also been reported in the ejecta beyond the crater rim, where the covering suevite heated the fluid-rich Bunte Breccia, leading to a devolatilization and the generation of degassing pipes within the suevite (Caudill et al., 2021; Pietrek & Kenkmann, 2016; Sapers et al., 2017). The interaction of water with the hot impactites produced a system of convective fluids capable of dissolving, transporting, and precipitating minerals (e.g., Newsom et al., 1986, 2005;

Osinski, 2005; Osinski et al., 2001), including magnetic minerals as shown in our study. According to our findings at the Aumühle quarry, the hydrothermal activity was spatially heterogeneous, not very pervasive, and confined to the vicinity within the Bunte Breccia up to the contact with the suevite. The exact temperature of the hydrothermal fluids is difficult to determine in our study, as CRM can form from high to near ambient temperatures (Dunlop & Özdemir, 2015). Osinski (2005) suggested that the main stage of hydrothermal activity in the ejecta outside the crater was about 100–130°C based on the alteration products of calcite and montmorillonite. This is indicated by Phase 3 in Figure 10, where high-temperature hydrothermal activity was followed by a prolonged cooling period (Arp et al., 2019; Naumov, 2005; Sapers et al., 2017).

5.4. Comparison With Allochthonous Rocks of Comparable Lithologies

We studied four widely distributed outcrops of allochthonous crystalline basement blocks and two autochthonous sedimentary outcrops in and around the impact structure. Most samples displayed unstable remanence directions, except for at Wennenberg and Wengenhausen (Figure 1a). The ejected granitoid block at Wengenhausen (e.g., Sturm et al., 2015) yielded two clear and consistent magnetization components: one oriented $D = 192.5°$, $I = -60.5°$ ($\alpha_{95} = 4.6°$) (Ries Component) between 132 and 422°C that did not trend toward the origin on orthogonal plots and another oriented ca. $D = 249.7$, $I = 46.1°$ ($\alpha_{95} = 6.2°$) that decays toward the origin by ca. 580°C (Figures 6c and 6d). Microscopic investigations reveal the presence of fractures in the granitoids (Figures S6c, S6d in Supporting Information S1), which probably occurred due to the Ries impact event. No shock effects were found in this outcrop. Our interpretation is that the Wengenhausen granitoid was heated to ca. 422°C during excavation and then cooled in the Ries field. The higher temperature component is likely a primary magnetization component in magnetite; not knowing the original paleohorizontal precludes testing this further.

Granodiorite from Wennenberg yielded an average direction of $D = 218.3°$, $I = -43.7°$ ($\alpha_{95} = 6.5°$, $N = 27$) unblocked by thermal demagnetization up to ca. 550°C, whose trajectories did not decay to the origin (Figures 6h and 6i). This component was observed in 27 of 33 demagnetized samples collected over ca. 30 m in an abandoned quarry atop a hill marking a topographic high on the rim of the central ring (Figure 1a). The exact age of the granodiorite is unknown, but gneisses and granites elsewhere in the Ries crater yield monazite U-Pb dates from 370 to 320 Ma, consistent with Variscan metamorphic and magmatic events (Horn et al., 1985; Tartèse et al., 2022). Expected Variscan paleolatitudes from the European apparent polar wander path place Ries at low (5–10°S) latitudes in the southern hemisphere (Torsvik et al., 2008; Van der Voo, 1993). The south and up direction implies a northern hemisphere origin with a paleolatitude of ∼27°N; moreover, the average paleomagnetic direction lies close to the expected Ries direction.

An impact-related overprint implies that Wennenberg underwent a structural reorientation after the remanence was locked-in. This scenario predicts long cooling times given the massive nature of the granodiorite body, which is consistent with the relatively high degree of scatter ($k = 17.2$; Figure 4k). However, paleomagnetic directions in the Ries suevite are tightly grouped, with no evidence for structural modification throughout the crater by the time they cooled to ca. 580°C, making it difficult to argue for ductile or brittle readjustments long after crater formation. This appears to be true for craters of all ages and sizes (Gilder et al., 2018). Few paleomagnetic data come from basement rocks near the center of impact structures. An exception is the 85 km diameter Manicouagan structure, whose central peak has the same direction as the surrounding impact melts (Eitel et al., 2016). Alternatively, there are two other potential explanations for the observed magnetization directions in the Wennenberg block. One possibility is that the block retained an inherited pre-existing remanence, and during the crater formation, it rotated. Another possibility is that new magnetic minerals were formed through hydrothermal alteration processes, similar to the sedimentary clasts in the Bunte Breccia at Aumühle. In this case, the remanence would have a chemical origin. As no shock effects are recorded from this locality, the latter might be more likely. In sum, we are not certain about the timing of remanence acquisition and structure modification, but the results suggest that impact heating of the basement rocks seven km from the crater center could be as high as 500–550°C (Figure 1a).

5.5. Implications for the Origin and Evolution of Life

Hydrothermal vents that spew hot, mineral-rich fluids on the ocean floor have been proposed as possible sites for the origin of life. This unique environment can provide the necessary conditions for life to emerge, including a source of energy, chemical compounds, and protection from harmful ultraviolet radiation (e.g., Georgieva et al., 2021; Russell & Hall, 1997). Meteorite impacts might have also facilitated the origin of life on Earth. For

example, in the Haughton impact structure, Cockell et al. (2002) found that the cyanobacterial colonization in heavily shocked gneissic crystalline basement rocks was greater than in unshocked gneisses. Impact-induced hydrothermal systems have been proposed to provide an environment to build and sustain life for extended time periods (Osinski et al., 2013; Osinski et al., 2020). So too would be the Bunte Breccia horizon near the contact with suevite, which contains the chemical and thermal gradients needed to provide the energy and nutrients for life to form, as demonstrated in our study. A suevite cover, analogous to the deep sea, would be very efficient as sheltering nascent life from ultraviolet radiation. Our study in the 26 km-diameter Ries impact structure limits this to ~139 kyr; however, hydrothermal activity at the much larger Chicxulub impact structure might have lasted much longer (Kring et al., 2020).

6. Conclusions

Our observations at the Aumühle quarry, summarized in Figure 10, suggest that Bunte Breccia was chemically altered and locally heated by the overlying suevite. Basement clasts in the Bunte Breccia possess stable remanent magnetizations with randomly oriented paleomagnetic directions. Most of those clasts have hematite as remanence carriers, although a few have magnetite. Reheating the hematite-bearing clasts to 300°C in an applied field of 50 µT was ineffective at generating a partial thermal remanent magnetization, whereas it was effective for magnetite-bearing clasts. These results suggest that the magnetization of the randomized clasts was blocked before rotation and that the temperature in the hydrothermal system at the contact zone was not more than 300°C, because the random clasts CB06 and CB09 containing magnetite were likely not partially thermally overprinted. Many magnetite-bearing clasts are carbonate-rich sediments that recorded the magnetic field at the time of impact. The magnetic minerals in those clasts grew chemically with remanences that became locked in as the grains grew through the blocking volume (CRM). This process can occur at relatively low temperatures, yet the unblocking temperatures will persist up to the Curie temperatures of the ferrimagnetic phases carrying the remanence. The rotated clasts provide unequivocal proof for turbulent emplacement of the ejecta blanket.

Suevite lying tens of cm from the contact with the Bunte Breccia possesses very stable and tightly grouped paleomagnetic directions carried by magnetite. Approaching the contact, the magnetite is partially altered to hematite and/or hematite is newly precipitated from a fluid. Hematite-bearing suevite also possesses the Ries direction, yet with more scatter, suggesting longer cooling times recorded more secular variation of the ambient magnetic field. This observation suggests the fluids at the contact were warm, oxidizing, and sustained for longer times than it took for the overlying suevite to cool. Degassing pipes in the suevite indicate convective cooling. The third stage represents low-temperature (≤100°C) hydrothermal activity during which chemical alteration of the clasts continued over a prolonged period at most up until the end of reversed chron C5ADr, for a maximum possible duration of 139 kyr. Although this latter point is more speculative, none of the hematite-bearing rocks have normal polarity, and no other data exists to constrain the duration of hydrothermal activity more precisely.

Basement rocks outside of Aumühle have much different magnetic properties than the basement clasts in the Bunte Breccia at Aumühle as well as the basement clasts in the suevite. The Gundelsheim and Harburg limestones and Maihingen granite have weak magnetizations with uninterpretable demagnetization spectra; the Tiefenthal amphibolites had highly variable magnetization behavior with no coherent magnetization component. In contrast, granitoids near or on the inner ring were partially to nearly fully thermally reset (422°C in Wengenhausen, 475–550°C in Wennenberg) by cratering. This would either indicate shock heating (however, no shock effects are recorded in the investigated samples) or hydrothermal alteration during or after excavation of the target rocks.

Data Availability Statement

Stepwise demagnetization and rock magnetic data are available on the MagIC portal (Sleptsova et al., 2024): https://earthref.org/MagIC/19984.

References

Abadian, M. (1972). Petrographie, Stoßwellenmetamorphose und Entstehung polymikter kristalliner Breccien im Nördlinger Ries. *Contributions to Mineralogy and Petrology*, *35*(3), 245–262. https://doi.org/10.1007/BF00371219

Arp, G., Kolepka, C., Simon, K., Karius, V., Nolte, N., & Hansen, B. T. (2013). New evidence for persistent impact-generated hydrothermal activity in the Miocene Ries impact structure, Germany. *Meteoritics & Planetary Science*, *48*(12), 2491–2516. https://doi.org/10.1111/maps.12235

Arp, G., Reimer, A., Simon, K., Sturm, S., Wilk, J., Kruppa, C., et al. (2019). The Erbisberg drilling 2011: Implications for the structure and postimpact evolution of the inner ring of the Ries impact crater. *Meteoritics & Planetary Science*, *54*(10), 2448–2482. https://doi.org/10.1111/maps.13293

Baranyi, I. (1980). Untersuchungen über die Veränderungen von Sedimentgesteinseinschlüssen im Suevit des Nördlinger Rieses. *Beiträge zur naturkundlichen Forschung Südwest-Deutschlands*, *39*, 37–56.

Carporzen, L., Weiss, B. P., Gilder, S. A., Pommier, A., & Hart, R. J. (2012). Lightning remagnetization of the Vredefort impact crater: No evidence for impact-generated magnetic fields. *Journal of Geophysical Research*, *117*(E1), 1–17. https://doi.org/10.1029/2011JE003919

Caudill, C., Osinski, G. R., Greenberger, R. N., Tornabene, L. L., Longstaffe, F. J., Flemming, R. L., & Ehlmann, B. L. (2021). Origin of the degassing pipes at the Ries impact structure and implications for impact-induced alteration on Mars and other planetary bodies. *Meteoritics & Planetary Science*, *56*(2), 1–422. https://doi.org/10.1111/maps.13600

Cockell, C. S., Lee, P., Osinski, G. R., Horneck, G., & Broady, P. (2002). Impact-induced microbial endolithic habitats. *Meteoritics & Planetary Science*, *37*(10), 1287–1298. https://doi.org/10.1111/j.1945-5100.2002.tb01029.x

Collins, G. S., Melosh, H. J., & Osinski, G. R. (2012). The impact-cratering process. *Elements*, *8*(1), 25–30. https://doi.org/10.2113/gselements.8.1.25

Deenen, M. H. L., Langereis, C. G., van Hinsbergen, D. J. J., & Biggin, A. J. (2011). Geomagnetic secular variation and the statistics of palaeomagnetic directions. *Geophysical Journal International*, *186*(2), 509–520. https://doi.org/10.1111/j.1365-246x.2011.05050.x

Dellefant, F., Trepmann, C. A., Schmahl, W. W., Gilder, S. A., Sleptsova, I. V., & Kaliwoda, M. (2023). Ilmenite phase transformations in suevite from the Ries impact structure (Germany) record evolving temperature, pressure, and oxygen fugacity conditions. *American Mineralogist*. https://doi.org/10.2138/am-2023-8985

Di Vincenzo, G. (2022). High precision multi-collector $^{40}Ar/^{39}Ar$ dating of moldavites (Central European tektites) reconciles geochronological and paleomagnetic data. *Chemical Geology*, *608*, 121026. https://doi.org/10.1016/j.chemgeo.2022.121026

Draeger, U., Prévot, M., Poidras, T., & Riisager, J. (2006). Single-domain chemical, thermochemical and thermal remanences in a basaltic rock. *Geophysical Journal International*, *166*(1), 12–32. https://doi.org/10.1111/j.1365-246X.2006.02862.x

Dunlop, D. J., & Özdemir, Ö. (1997). *Rock magnetism: Fundamentals and frontiers*. Cambridge University Press. https://doi.org/10.1017/CBO9780511612794

Dunlop, D. J., & Özdemir, Ö. (2015). Magnetizations in rocks and minerals. In G. Schubert (Ed.), *Treatise on geophysics* (Vol. 5 Geomagnetism, 2nd ed., pp. 255–308). https://doi.org/10.1016/b978-0-444-53802-4.00102-0

Eitel, M., Gilder, S. A., Spray, J., Thompson, L., & Pohl, J. (2016). A paleomagnetic and rock magnetic study of the Manicouagan impact structure: Implications for crater formation and geodynamo effects. *Journal of Geophysical Research: Solid Earth*, *121*(2), 436–454. https://doi.org/10.1002/2015JB012577

Fisher, R. (1953). Dispersion on a sphere. *Proceedings of the Royal Society of London. Series A. Mathematical and Physical Sciences, Royal Society*, *217*(1130), 295–305. https://doi.org/10.1098/rspa.1953.0064

Gall, H., Müller, D., & Stöffler, D. (1975). Verteilung, Eigenschaften und Entstehung der Auswurfmassen des Impaktkraters Nördlinger Ries. *Geologische Rundschau*, *64*(1), 915–947. https://doi.org/10.1007/BF01820704

Georgieva, M. N., Little, C. T. S., Maslennikov, V. V., Glover, A. G., Ayupova, N. R., & Herrington, R. J. (2021). The history of life at hydrothermal vents. *Earth-Science Reviews*, *217*, 103602. https://doi.org/10.1016/j.earscirev.2021.103602

Gilder, S. A., Pohl, J., & Eitel, M. (2018). *Magnetic signatures of terrestrial meteorite impact craters: A summary*. In H. Lühr, J. Wicht, S. Gilder, & M. Holschnieider (Eds.), *Magnetic fields in the solar system* (Vol. 448). Springer Verlag. https://doi.org/10.1007/978-3-319-64292-5

Heap, M. J., Gilg, H. A., Byrne, P. K., Wadsworth, F. B., & Reuschlé, T. (2020). Petrophysical properties, mechanical behaviour, and failure modes of impact melt-bearing breccia (suevite) from the Ries impact crater (Germany). *Icarus*, *349*, 113873. https://doi.org/10.1016/j.icarus.2020.113873

Heap, M. J., Gilg, H. A., Hess, K.-U., Mertens, L., Pösges, G., & Reuschlé, T. (2020). Conservation and restoration of St. George's church (Nördlingen, Germany), a 15th century Gothic church built using suevite from the Ries impact crater. *Journal of Cultural Heritage*, *41*, 256–263. https://doi.org/10.1016/j.culher.2019.07.002

Horn, P., Müller-Sohnius, D., Köhler, H., & Graup, G. (1985). Rb-Sr systematics of rocks related to the Ries Crater, Germany. *Earth and Planetary Science Letters*, *75*(4), 384–392. https://doi.org/10.1016/0012-821X(85)90181-5

Hörz, F., & Banholzer, G. S. (1980). Deep-seated target materials in the continuous deposits of the Ries Crater, Germany. In J. J. Papike & R. B. Merrill (Eds.), *Proceedings of the Conference on Lunar Highlands Crust* (pp. 211–231). Pergamon Press.

Hörz, F., Ostertag, R., & Rainey, D. A. (1983). Bunte Breccia of the Ries: Continuous deposits of large impact craters. *Reviews of Geophysics*, *21*(8), 1667–1725. https://doi.org/10.1029/RG021i008p01667

Huang, W., Lippert, P. C., Zhang, Y., Jackson, M. J., Dekkers, M. J., Li, J., et al. (2017). Remagnetization of carbonate rocks in southern Tibet: Perspectives from rock magnetic and petrographic investigations. *Journal of Geophysical Research: Solid Earth*, *122*(4), 2434–2456. https://doi.org/10.1002/2017JB013987

Hüttner, R. (1969). Bunte Trümmermassen und Suevit. *Geologica Bavarica*, *61*, 142–200.

Hüttner, R., & Schmidt-Kaler, H. (1999). Erläuterungen zur geologischen Karte des Rieses 1:50 000. *Geologica Bavarica*, *104*, 7–76.

Kenkmann, T. (2021). The terrestrial impact crater record: A statistical analysis of morphologies, structures, ages, lithologies, and more. *Meteoritics & Planetary Science*, *56*(5), 1024–1070. https://doi.org/10.1111/maps.13657

Kim, W., Doh, S., Yu, Y., Lee, J., & Suk, D. (2009). Hydrothermal fluid-controlled remagnetization of sedimentary rocks in Korea: Tectonic importance of pervasive Tertiary remagnetization. *Tectonophysics*, *474*(3–4), 684–695. https://doi.org/10.1016/j.tecto.2009.05.014

Kirschvink, J. (1980). The least-squares line and plane and the analysis of palaeomagnetic data. *Geophysical Journal of the Royal Astronomical Society*, *62*(3), 699–718. https://doi.org/10.1111/j.1365-246X.1980.tb02601.x

Kobayashi, K. (1959). Chemical remanent magnetization of ferromagnetic minerals and its application to rock magnetism. *Journal of Geomagnetism and Geoelectricity*, *10*(3), 99–117. https://doi.org/10.5636/jgg.10.99

Koch, S. A., Gilder, S. A., Pohl, J., & Trepmann, C. (2012). Geomagnetic field intensity recorded after impact in the Ries meteorite crater, Germany. *Geophysical Journal International*, *189*(1), 383–390. https://doi.org/10.1111/j.1365-246X.2012.05399.x

Kowitz, A., Güldemeister, N., Reimold, W. U., Schmitt, R. T., & Wünnemann, K. (2013). Diaplectic quartz glass and SiO_2 melt experimentally generated at only 5 GPa shock pressure in porous sandstone: Laboratory observations and meso-scale numerical modeling. *Earth and Planetary Science Letters*, *384*, 17–26. https://doi.org/10.1016/j.epsl.2013.09.021

Kring, D. A., Tikoo, S. M., Schmieder, M., Riller, U., Rebolledo-Vieyra, M., Simpson, S. L., et al. (2020). Probing the hydrothermal system of the Chicxulub impact crater. *Science Advances*, *6*(22). https://doi.org/10.1126/sciadv.aaz3053

Kurosawa, K., Ono, H., Niihara, T., Sakaiya, T., Kondo, T., Tomioka, N., et al. (2022). Shock recovery with decaying compressive pulses: Shock effects in calcite ($CaCO_3$) around the Hugoniot elastic limit. *Journal of Geophysical Research: Planets*, *127*(6). https://doi.org/10.1029/2021JE007133

Kuzina, D. M., Gattacceca, J., Bezaeva, N., Badjukov, D., Rochette, P., Quesnel, Y., et al. (2022). Paleomagnetic study of impactites form the Karla impact structure suggest protracted post-impact hydrothermalism. *Meteoritics & Planetary Science*, *57*(10), 1846–1860. https://doi.org/10.1111/maps.13906

Langenhorst, F., Boustie, M., Deutsch, A., Hornemann, U., Matignon, C., Migault, A., & Romain, J. P. (2003). Experimental techniques for the simulation of shock metamorphism: A case study on calcite. In *High-pressure shock compression of solids V* (pp. 1–27). Springer. https://doi.org/10.1007/978-1-4613-0011-3_1

Larson, E. E., Walker, T. R., Patterson, P. E., Hoblitt, R. P., & Rosenbaum, J. G. (1982). Paleomagnetism of the Moenkopi Formation, Colorado Plateau: Basis for long-term model of acquisition of chemical remanent magnetism in red beds. *Journal of Geophysical Research*, *87*(B2), 1081–1106. https://doi.org/10.1029/JB087iB02p01081

Lowrie, W. (1990). Identification of ferromagnetic minerals in a rock by coercivity and unblocking temperature properties. *Geophysical Research Letters*, *17*(2), 159—162–162. https://doi.org/10.1029/GL017i002p00159

McFadden, P. L., & Lowes, F. J. (1981). The discrimination of mean directions drawn from Fisher distributions. *Geophysical Journal of the Royal Astronomical Society*, *67*(1), 19–33. https://doi.org/10.1111/j.1365-246X.1981.tb02729.x

Melosh, H. J. (1989). *Impact cratering: A geologic process*. Clarendon Press.

Muttik, N., Kirsimäe, K., & Vennemann, T. W. (2010). Stable isotope composition of smectite in suevites at the Ries crater, Germany: Implications for hydrous alteration of impactites. *Earth and Planetary Science Letters*, *299*(1–2), 190–195. https://doi.org/10.1016/j.epsl.2010.08.034

Naumov, M. V. (2005). Principal features of impact-generated hydrothermal circulation systems: Mineralogical and geochemical evidence. *Geofluids*, *5*(3), 165–184. https://doi.org/10.1111/j.1468-8123.2005.00092.x

Néel, L. (1949). Théorie du traînage magnétique des ferromagnétiques en grains fins avec applications aux terres cuites. *Annales de Geophysique*, *5*, 99–136.

Newsom, H., Graup, G., Sewards, T., & Keil, K. (1986). Fluidization and hydrothermal alteration of the suevite deposit at the Ries crater, west Germany, and implications for Mars. *Journal of Geophysical Research*, *91*(B13), E239–E251. https://doi.org/10.1029/JB091iB13p0E239

Newsom, H., Nelson, M. J., & Shearer, C. K. (2005). *Hydrothermal processes and mobile element transport in Martian impact craters—Evidence from terrestrial analogue craters. Proceedings workshop on the role of volatiles and atmospheres on martian impact craters. LPI contribution 1273* (pp. 1–2). Lunar and Planetary Institute.

Oberbeck, V. R. (1975). The role of ballistic erosion and sedimentation in lunar stratigraphy. *Reviews of Geophysics*, *13*(2), 337–362. https://doi.org/10.1029/RG013i002p00337

Ogg, J. G. (2020). *Geomagnetic polarity time scale, in geologic time scale*. In F. M. Gradstein, J. G. Ogg, M. D. Schmitz, & G. M. Ogg (Eds.), *Geologic time scale 2020* (Vol. 1, pp. 159–192). Elsevier. https://doi.org/10.1016/B978-0-12-824360-2.00005-X

Osinski, G. R. (2004). Impact melt rocks from the Ries structure, Germany: An origin as impact melt flows? *Earth and Planetary Science Letters*, *226*(3–4), 529–543. https://doi.org/10.1016/j.epsl.2004.08.012

Osinski, G. R. (2005). Hydrothermal activity associated with the Ries impact event, Germany. *Geofluids*, *5*(3), 202–220. https://doi.org/10.1111/j.1468-8123.2005.00119.x

Osinski, G. R., Cockell, C. S., Pontefract, A., & Sapers, H. M. (2020). The role of meteorite impacts in the origin of life. *Astrobiology*, *20*(9), 1121–1149. https://doi.org/10.1089/ast.2019.2203

Osinski, G. R., Grieve, R. A. F., Ferrière, L., Losiak, A., Pickersgill, A. E., Cavosie, A. J., et al. (2022). Impact Earth: A review of the terrestrial impact record. *Earth-Science Reviews*, *232*, 104112. https://doi.org/10.1016/j.earscirev.2022.104112

Osinski, G. R., Spray, J. G., & Lee, P. (2001). Impact-induced hydrothermal activity within the Haughton impact structure, arctic Canada: Generation of a transient, warm, wet oasis. *Meteoritics & Planetary Science*, *36*(5), 731–745. https://doi.org/10.1111/j.1945-5100.2001.tb01910.x

Osinski, G. R., Tornabene, L. L., Banerjee, N. R., Cockell, C. S., Flemming, R. L., Izawa, M., et al. (2013). Impact-generated hydrothermal systems on Earth and Mars. *Icarus*, *224*(2), 347–363. https://doi.org/10.1016/j.icarus.2012.08.030

Osinski, G. R., Tornabene, L. L., & Grieve, R. A. F. (2011). Impact ejecta emplacement on terrestrial planets. *Earth and Planetary Science Letters*, *310*(3–4), 167–181. https://doi.org/10.1016/j.epsl.2011.08.012

Parnell, J., Taylor, C. W., Thackrey, S., Osinski, G. R., & Lee, P. (2010). Permeability data for impact breccias imply focussed hydrothermal fluid flow. *Journal of Geochemical Exploration*, *106*(1–3), 171–175. https://doi.org/10.1016/j.gexplo.2009.12.002

Pietrek, A., & Kenkmann, T. (2016). Ries Bunte Breccia revisited: Indications for the presence of water in Itzing and Otting drill cores and implications for the emplacement process. *Meteoritics & Planetary Science*, *51*(7), 1203–1222. https://doi.org/10.1111/maps.12656

Pohl, J. (1965). Die Magnetisierung der Suevite des Rieses. *Neues Jahrbuch für Mineralogie - Monatshefte*, *9*, 268–276.

Pohl, J., Poschlod, K., Reimold, W. U., Meyer, C., & Jacob, J. (2010). *Ries crater, Germany: The Enkingen magnetic anomaly and associated drill core SUBO 18*. In R. L. Gibson & W. U. Reimold (Eds.), *Large meteorite impacts and planetary evolution IV* (Vol. 465, pp. 141–163). Geological Society of America Special Paper. https://doi.org/10.1130/2010.2465(10)

Pohl, J., Stöffler, D., Gall, H., & Ernstson, K. (1977). The Ries impact crater. In D. J. Roddy, R. O. Pepin, & R. B. Merrill (Eds.), *Impact and explosion cratering* (pp. 343–404). Pergamon.

Pullaiah, G., Irving, E., Buchan, K. L., & Dunlop, D. J. (1975). Magnetization changes caused by burial and uplift. *Earth and Planetary Science Letters*, *28*(2), 133–143. https://doi.org/10.1016/0012-821X(75)90221-6

Rocholl, A., Schaltegger, U., Gilg, H. A., Wijbrans, J., & Böhme, M. (2018). The age of volcanic tuffs from the upper Freshwater Molasse (north Alpine Foreland basin) and their possible use for tephrostratigraphic correlations across Europe for the Middle Miocene. *International Journal of Earth Sciences*, *107*(2), 387–407. https://doi.org/10.1007/s00531-017-1499-0

Russell, M. J., & Hall, A. J. (1997). The emergence of life from iron monosulphide bubbles at a submarine hydrothermal redox and pH front. *Journal of the Geological Society*, *154*(3), 377–402. https://doi.org/10.1144/gsjgs.154.3.0377

Sapers, H. M., Osinski, G. R., Flemming, R. L., Buitenhuis, E., Banerjee, N. R., Tornabene, L., et al. (2017). Evidence for a spatially extensive hydrothermal system at the Ries impact structure, Germany. *Meteoritics & Planetary Science*, *52*(2), 351–371. https://doi.org/10.1111/maps.12796

Seybold, L., Trepmann, C. A., Hölzl, S., Pollok, K., Langenhorst, F., Dellefant, F., & Kaliwoda, M. (2023). Twinned calcite as an indicator of high differential stresses and low shock pressure conditions during impact cratering. *Meteoritics & Planetary Science*, *58*(9), 1287–1305. https://doi.org/10.1111/maps.14056

Sleptsova, I. V., Gilder, S. A., Dellefant, F., Trepmann, C. A., Ahanin, N., & Pohl, J. (2024). Thermal and structural history of impact ejecta deposits, Ries impact structure, Germany [Dataset]. MagIC. https://doi.org/10.7288/V4/MAGIC/19984

Stöffler, D., Artemieva, N. A., & Pierazzo, E. (2002). Modeling the Ries-Steinheim impact event and the formation of the moldavite strewn field. *Meteoritics & Planetary Science*, *37*(12), 1893–1907. https://doi.org/10.1111/j.1945-5100.2002.tb01171.x

Stöffler, D., Artemieva, N. A., Wünnemann, K., Reimold, W. U., Jacob, J., Hansen, B. K., & Summerson, I. A. T. (2013). Ries crater and suevite revisited—Observations and modeling Part I: Observations. *Meteoritics & Planetary Science*, *48*(4), 515–589. https://doi.org/10.1111/maps.12086

Stöffler, D., Hamann, C., & Metzler, K. (2018). Shock metamorphism of planetary silicate rocks and sediments: Proposal for an updated classification system. *Meteoritics & Planetary Science*, *53*(1), 5–49. https://doi.org/10.1111/maps.12912

Sturm, S., Kenkmann, T., Willmes, M., Pösges, G., & Hiesinger, H. (2015). The distribution of megablocks in the Ries crater, Germany: Remote sensing, field investigation, and statistical analyses. *Meteoritics & Planetary Science*, *50*(1), 141–171. https://doi.org/10.1111/maps.12408

Sun, W. W., & Jackson, M. (1994). Scanning electron microscopy and rock magnetic studies of magnetic carriers in remagnetized early Paleozoic carbonates from Missouri. *Journal of Geophysical Research*, *99*(B2), 2935–2942. https://doi.org/10.1029/93JB02761

Tartèse, R., Endley, S., & Joy, K. H. (2022). U-Pb dating of zircon and monazite from the uplifted Variscan crystalline basement of the Ries impact crater. *Meteoritics & Planetary Science*, *57*(4), 830–849. https://doi.org/10.1111/maps.13798

Torsvik, T. H., Müller, R. D., Van der Voo, R., Steinberger, B., & Gaina, C. (2008). Global plate motion frames: Toward a unified model. *Reviews of Geophysics*, *46*(3), RG3004. https://doi.org/10.1029/2007RG000227

Van der Voo, R. (1993). *Paleomagnetism of the Atlantic, Tethys, and Iapetus oceans*. Cambridge University Press.

Volk, M. V. R. (2016). *Influence of pressure, temperature and composition on magnetic recording in meteorites (Doctoral dissertation)*. Ludwig Maximilians University. Retrieved from Electronic Theses of LMU Munich Retrieved from https://edoc.ub.uni-muenchen.de/19824/

Von Engelhardt, W., & Graup, G. (1984). Suevite of the Ries crater, Germany: Source rocks and implications for cratering mechanics. *Geologische Rundschau*, *73*(2), 447–481. https://doi.org/10.1007/BF01824968

Von Engelhardt, W. (1972). Shock produced rock glasses from the Ries crater. *Contributions to Mineralogy and Petrology*, *36*(4), 265–292. https://doi.org/10.1007/bf00444336

Von Engelhardt, W. (1990). Distribution, petrography and shock metamorphism of the ejecta of the Ries crater in Germany—A review. *Tectonophysics*, *171*(1–4), 259–273. https://doi.org/10.1016/0040-1951(90)90104-G

Von Engelhardt, W., Arndt, J., Fecker, B., & Pankau, H. (1995). Suevite breccia from the Ries crater, Germany: Origin, cooling history and devitrification of impact glasses. *Meteoritics & Planetary Science*, *30*(3), 279–293. https://doi.org/10.1111/j.1945-5100.1995.tb01126.x

Von Engelhardt, W., Stöffler, D., & Schneider, W. (1969). Petrologische Untersuchungen im Ries. *Geologica Bavarica*, *61*, 229–295.

Wack, M., & Gilder, S. (2012). The SushiBar: An automated system for paleomagnetic investigations. *Geochemistry, Geophysics, Geosystems*, *13*(3). https://doi.org/10.1029/2011GC003985

Walker, T. R., Larson, E. E., & Hoblitt, R. P. (1981). Nature and origin of hematite in the Moenkopi formation (Triassic), Colorado plateau: A contribution to the origin of magnetism in red beds. *Journal of Geophysical Research*, *86*(B1), 317–333. https://doi.org/10.1029/JB086iB01p00317

Watson, G. S. (1956). A test for randomness of directions. *Geophysical Journal International*, *7*(s4), 160–161. https://doi.org/10.1111/j.1365-246X.1956.tb05561.x

Weil, A. B., & Van der Voo, R. (2002). Insights into the mechanism for orogen-related carbonate remagnetization from growth of authigenic Fe-oxide: A scanning electron microscopy and rock magnetic study of Devonian carbonates from northern Spain. *Journal of Geophysical Research*, *107*(B4). https://doi.org/10.1029/2001JB000200

Zylberman, W., Quesnel, Y., Rochette, P., Osinski, G. R., Marion, C., & Gattacceca, J. (2017). Hydrothermally-enhanced magnetization at the center of the Haughton impact structure? *Meteoritics and Planetary Science*, *52*(10), 2147–2165. https://doi.org/10.1111/maps.12917